

STABILITY ANALYSIS AND CONTROL DESIGN
FOR UNCERTAIN AND TIME-DELAY SYSTEMS

By

SALEH A. AL-SHAMALI

A DISSERTATION PRESENTED TO THE GRADUATE SCHOOL
OF THE UNIVERSITY OF FLORIDA IN PARTIAL FULFILLMENT
OF THE REQUIREMENTS FOR THE DEGREE OF
DOCTOR OF PHILOSOPHY

UNIVERSITY OF FLORIDA

2004

Copyright 2004
by
Saleh A. Al-Shamali

I dedicate this work to my parents and my wife Muna.

ACKNOWLEDGMENTS

I wish to express my deep gratitude to my advisors, Dr. Haniph Latchman and Dr. Oscar Crisalle, for their support and guidance during my Ph.D. study. They gave me a lot of freedom and flexibility to choose my research topic. I am thankful for their encouragement which gives me confidence as I begin my career in academia as an assistant Professor, shortly after I graduate with my Ph.D.

I also wish to thank Dr. Tan Wong and Dr. Norman Fitz-Coy for serving on my committee, and for providing constructive ideas to further develop my research.

I am very thankful to Dr. William Hager and Dr. Sergi Pilyugin for their help on some of the mathematical difficulties I ran into during my research.

I would also like to thank my List lab colleagues, in particular, Dr. Baowei Ji, who offered his help and shared his extensive knowledge in the area of controls with me, and Mr. Minkyu Lee for his recognized role in administrating the List lab, and for taking the time to solve the many technical problems I ran into while he worked on his Ph.D. dissertation. I also wish to thank my List lab colleagues, Mr. Yu-Ju Lin, Mr. Kartikeya Tripathi, Mr. Suman Srinivasan, and the rest. I had a wonderful time and enjoyed being around them.

I am grateful to my parents, sisters, and brothers back in Kuwait for their support, and to my wife for standing behind me and for taking a long leave from her job to stay with me and take care of our son, Mohammed. My family has always been a source of inspiration and support for me throughout the course of my Ph.D. research.

TABLE OF CONTENTS

	<u>Page</u>
ACKNOWLEDGMENTS	iv
LIST OF FIGURES	vii
ABSTRACT	ix
CHAPTER	
1 INTRODUCTION	1
1.1 Robustness Analysis	1
1.2 Sliding Mode Control	2
1.3 Bilinear Systems	3
1.4 Thesis Structure	3
2 THE NYQUIST ROBUST SENSITIVITY MARGIN	5
2.1 Introduction	5
2.2 Background	7
2.3 The Nyquist Robust Sensitivity Margin	11
2.4 Application to Systems with Affine Uncertainty Structure	16
2.5 Examples	21
2.5.1 Example 1	21
2.5.2 Example 2	22
2.5.3 Example 3	24
2.6 Conclusions	26
2.7 Supplementary Calculation Algorithms	27
2.7.1 Supporting Circle of an Arc	27
2.7.2 Minimum Distance between a Line and a Point	28
2.7.3 Identifying Points on the Arc	29
3 SLIDING MODE CONTROL FOR TIME-DELAY SYSTEMS	30
3.1 Introduction	30
3.2 Problem Formulation	32
3.3 Switching Function and Control Law Design	33
3.4 Existence of a Sliding Mode	35
3.5 System Stability	36
3.6 Example	41
3.7 Conclusions	42

4	STABILIZATION OF TIME-DELAY BILINEAR SYSTEMS	45
4.1	Introduction	45
4.2	Problem Statement	46
4.3	Preliminary Results	47
4.4	Main Result	54
4.5	Example	57
4.6	Conclusions	58
4.7	Further Analysis of the System in Lemma 1	60
5	FUTURE WORK AND DISCUSSIONS	63
5.1	Problem 1 : Sliding Mode Control for a Delayed Bilinear System	63
5.2	Problem 2 : Extending the NRSM	63
	APPENDIX	66
A	DERIVATION FOR THE REACHING TIME	66
B	DERIVATION OF A BOUND USED IN CHAPTER 3	69
C	PROOF OF LEMMA 1 OF CHAPTER 4	70
D	PROOF OF CLAIM (i) OF LEMMA 1 OF CHAPTER 4	72
E	THE MATRIX MEASURE – DEFINITION AND PROPERTIES	74
F	THE COMPARISON THEOREM	75
	REFERENCES	76
	BIOGRAPHICAL SKETCH	81

LIST OF FIGURES

<u>Figure</u>	<u>page</u>
2.1 The uncertain system $g(s) = g_0(s) + \delta(s)$ in a unity-feedback configuration.	8
2.2 Uncertainty value sets at a frequency ω_i : (a) convex critical value set $\mathcal{V}_c(\omega_i)$, (b) nonconvex critical value set $\mathcal{V}(\omega_i)$. Both figures show the worst-sensitivity plant $g_s(j\omega_i)$, located closest to the point $-1 + j0$. 10	10
2.3 Illustration of the inverse-sensitivity circle of radius $\eta(\omega)$ introduced in definition (2.11).	12
2.4 The center z_0 and radius r of the supporting circle of the arc $A(p_1, p_2, p_3)$ are determined from the intersection of the auxiliary lines L_1 and L_2	18
2.5 Frame for the value set of system (2.23) at $\omega = 9$, and the corresponding inverse-sensitivity circle. The nominal plant $g_0(j\omega)$ is indicated by the '+' marker.	23
2.6 Value of $k_{N,s}(\omega)$ and $k_N(\omega)$ as a function of frequency for the first example.	23
2.7 Frame for the value set of system (2.25) at $\omega = 4.72$ and $\alpha = 1.86$. The nominal plant $g_0(j\omega)$ is indicated by the '+' marker.	25
2.8 Plot of the Nyquist robust sensitivity margin $k_{N,s} = [\max_{\omega} k_{N,s}(\omega)]$ as a function of the blow-up factor α . The parametric robust stability margin is $\bar{\alpha} = 1.89$, which corresponds to the value of the blow-up factor α that makes $k_{N,s}$ approximately equal to unity.	26
3.1 Trajectories for the states of the transformed system (a), the states of the original system (b), the control law (c), and the switching function (d).	43
3.2 Trajectories for the states of the transformed system (a), the states of the original system (b), the control law (c), and the switching function with approximation to the signum function (d).	44
4.1 Graphical interpretation of the differential equation of Lemma 2: (a) derivative graph, (b) solution curves	50

4.2	Plot of the trajectories of the system states.	59
4.3	Plot of the trajectories of the system states.	59
4.4	Graphical interpretation of the differential equation(4.4) for the case where $b > 0$: (a) derivative graph, (b) solution curves	61
4.5	Graphical interpretation of the differential equation(4.4) for the case where $b < 0$: (a) derivative graph, (b) solution curves	62
5.1	The negative feedback loop of the uncertain system $p(s)$ with a controller $c(s)$	64
5.2	The standard $M - \Delta$ loop for stability analysis.	65
5.3	A system with parametric uncertainty in the standard $M - \Delta$ loop. .	65
A.1	Plot of the switching function for $s(0) > 0$ (a), and $s(0) < 0$ (b). . . .	67

Abstract of Dissertation Presented to the Graduate School
of the University of Florida in Partial Fulfillment
of the Requirements for the Degree of
Doctor of Philosophy

STABILITY ANALYSIS AND CONTROL DESIGN
FOR UNCERTAIN AND TIME-DELAY SYSTEMS

By

Saleh A. Al-Shamali

December 2004

Chair: Haniph A. Latchman

Cochair: Oscar D. Crisalle

Major Department: Electrical and Computer Engineering

Uncertainty and time-delay in real systems constitute the two major challenges that face control engineers since both can contribute to instability or poor performance. In this dissertation three analysis and control design problems are addressed. These problems involve linear systems with parametric uncertainty structure, and linear and bilinear systems with time delay.

In the first problem, the Nyquist robust sensitivity margin is proposed as a scalar metric for robust stability and robust performance. The work was motivated by the critical direction theory (CDT) in which attention was given to plants that lie along the critical direction. The advantage of the new metric, however, is that it takes into account plants that are in close proximity to the critical point $-1 + j0$ but that do not lie along the critical direction. The approach introduced has therefore the advantage of capturing the worst case sensitivity as well as providing a more meaningful indication of robust stability. The concept has been applied successfully to a class of linear systems with affine uncertainty structure.

The second problem involves designing a sliding mode control (SMC) to stabilize a class of time-delay linear systems. The delay is assumed to exist in both the control variable as well as in the state vector. The system is first rendered input-delay free through an appropriate transformation. Then an SMC is designed for the state-delay system. Sufficient stability conditions ensuring the asymptotic stability of the closed-loop system have been derived.

The third problem addresses the stabilization of a class of time-delay bilinear systems. A state-feedback control law is designed to ensure the asymptotic stability of the delayed bilinear system. The work builds on two simple scalar systems and utilizes the results to prove a more complicated system. The analysis allowed us to obtain a bound on the maximum value of the delay that the system can tolerate. Furthermore, a region of attraction based on the initial condition of the systems states is established.

CHAPTER 1 INTRODUCTION

1.1 Robustness Analysis

The robustness analysis problem investigates the behavior of a dynamical system under uncertainty, namely, how the system stability and performance are influenced by the uncertainty. Many robust stability tools have been developed along the years, among which are the well-known scalar stability margins: the structured singular value $\mu(\omega)$ introduced by Doyle [17] and the multivariable stability margin given by Safanov $k_m(\omega)$ [46].

The critical direction theory introduced by Latchman and Crisalle [35] and later generalized by Baab *et al.* [2] also provides an effective tool for analyzing the robust stability of uncertain systems, namely, the Nyquist robust stability margin $k_N(\omega)$. The concept was applied successfully to a class of linear systems with affine and ellipsoidal uncertainty structure, and it works for the case of convex and non-convex value sets.

Uncertainties are classified depending on their source as non-parametric (unstructured) and parametric (structured) [7]. The non-parametric uncertainties do not have a well defined structure and are represented by a disk which over bounds the actual uncertainty. Therefore, this type of uncertainty description usually introduces conservatism. Examples of uncertainties that are represented as unstructured include non-linearities and un-modelled dynamics. Parametric uncertainties, on the other hand, have a structure that reflects the variation of the system parameters. Thus, they are less conservative. Examples of such uncertainties include interval and ellipsoidal uncertainty.

1.2 Sliding Mode Control

A variable structure system (VSS) is a dynamical system composed of distinct structures. A VSS switches between the different structures based on the value of its states and according to a switching logic which takes into account the desired properties in each structure. In fact, a variable structure system can have properties that are not existent in its individual structures [51].

A sliding mode control system (SMC) is a specific case of VSS in which the system trajectories exhibit a sliding behavior. The design of an SMC consists of two stages. The first stage is the design of a switching surface such that once the trajectories are confined to the surface the system demonstrates the desired properties (*i.e.*, tracking, regulation, etc.) The second stage involves the design of a control law that forces the trajectories into the sliding manifold (discontinuous control), and a linear feedback control that guarantees closed-loop stability (equivalent control). The latter is derived by setting the time derivative of the switching function equal to zero and solving for the control law. The former is proposed with appropriate gains to allow the system to overcome uncertainties.

The system motion in SMC runs through two phases. The first phase (reaching phase) is characterized by a fast motion. The system during this phase is robust against uncertainties (matched and unmatched) and external disturbances. This is mainly due to the discontinuous control law which acts as a high gain feedback control that counteracts high frequency signals. The second phase (sliding phase) is characterized by a slow motion. The system is however robust only against matched uncertainty.

The theory of sliding mode control has been covered comprehensively in the literature. Utkin [51] presents a survey for the early contributions in SMC. The survey by Hung et al. [26] presents a tutorial-like paper for variable structure control (VSC) with sliding mode. An interesting tutorial paper by DeCarlo et al. [16]

provides an introduction to variable structure control for multivariable nonlinear time-varying systems. Finally, a useful guide to SMC is also given by Young et al. [56].

1.3 Bilinear Systems

Bilinear systems occupy an intermediate level between linear and nonlinear systems in terms of their complexity. the general form of a bilinear systems is given as

$$\dot{x}(t) = Ax(t) + Bu(t) + Nx(t)u(t) \quad (1.1)$$

where it is clear that the control action enters the system linearly through the term $(Bu(t))$, and nonlinearly through the term $(Nx(t)u(t))$, hence the name bilinear system. A special form of the system (1.1) is the homogenous bilinear system

$$\dot{x}(t) = Ax(t) + Nx(t)u(t)$$

where the linear part is omitted. A formal definition of a bilinear system is given in Elliott [19]. Many natural as well as man-made systems can be represented as bilinear models [19, 39, 40]. Examples of bilinear systems can be found in economics, industrial processes, and biochemistry, just to mention a few.

1.4 Thesis Structure

The thesis is organized as follows. In Chapter 2, a new metric to the robust stability of closed-loop systems with affine uncertainty structure is presented. The new concept is motivated by the fact that the critical direction theory considers only plants that lie along the critical direction defined as the ray starting at the nominal plant and pointing towards the critical point $-1 + j0$. Hence, plants that are very close to the critical point but that do not lie on the critical ray are ignored. Therefore, the Nyquist robust sensitivity margin, $k_{N,s}$, is proposed to take into accounts such plants. Chapter 3 considers the stabilization of a class of time-delay linear systems

via sliding mode control. The delayed system is assumed to have a constant delay in both the input and the state. In Chapter 4, a state feedback control design for a class of bilinear systems with state-delay is presented. The stability conditions derived provide a bound on the system delay, and define an attraction region based on the initial condition. The future work proposed for consideration is presented in Chapter 5.

CHAPTER 2

THE NYQUIST ROBUST SENSITIVITY MARGIN

2.1 Introduction

The critical direction theory introduced by Latchman and Crisalle [35], Latchman *et al.* [36], and later generalized by Baab *et al.* [2] is an effective approach for analyzing the robust stability of uncertain systems with convex and non-convex uncertainty value sets. A key concept introduced by the theory is the Nyquist robust stability margin, $k_N(\omega)$, which provides a measure of robustness. The approach has proven useful in characterizing the robust stability of single-input/single-output systems with real affine parametric uncertainty, among others, and has recently been applied to the design of robustly stabilizing H_∞ controllers by identifying an appropriate weighting function for the controller sensitivity function [29, 30].

This chapter proposes an alternative robust-stability analysis which has the benefit of also capturing the concept of robust sensitivity, hence directly incorporating the notion of performance robustness. The resulting Nyquist robust sensitivity margin $k_{N,s}(\omega)$ is inspired on the critical direction theory framework, but is formulated to take into account in an explicit fashion the effect of the uncertain systems that have the worst-case sensitivity.

The earlier critical direction theory involving the margin $k_N(\omega)$ considers only a subset of the uncertain systems in the robustness analysis, namely, those uncertain systems whose image on the Nyquist plane lie along a pre-specified oriented line. Although the restricted critical-set of systems considered leads to non-conservative conditions for robust stability, the approach ignores all perturbed systems that have a poor sensitivity (*i.e.*, systems located close to the critical point $-1+j0$ on the Nyquist

plane) whenever these lie outside the oriented line. The new paradigm involving the margin $k_{N,s}(\omega)$ seeks to quantify the effect of the systems located closest to the critical point through the introduction of a sensitivity perturbation radius that is calculated at each frequency by solving an optimization program.

To illustrate the approach, the robust stability analysis proposed is developed for uncertain systems described by rational transfer functions with real affine parametric perturbations. More specifically, the numerator and denominator polynomials depend affinely on a set of real parameters that are known to belong to a given uncertainty description. A systematic algorithm for the calculation of $k_{N,s}(\omega)$ is developed by taking advantage of simple geometrical features adopted by the Nyquist-plane images of such systems [21]. The analysis is carried out in detail in Section 4.

The robust stability of the real affine uncertain systems considered in Section 4 can be analyzed using alternative approaches, for example, based on generalizations of Kharitonov's methodology [32]. In particular, one may adopt the approach in Barmish [3] which proposes a strict positivity condition that must be evaluated at a finite number of frequencies, or the box theorem [8], or the worst-edge algorithm of Sideris [48]. Furthermore, for the robust stability of interval plants, Wang [53] has shown that it suffices to check two vertices. Some results concerning the robust stability of control systems under unstructured as well as parametric uncertainty have been addressed in Chapellat [9]. These alternative results successfully reveal whether the system is robustly stable; however, in contrast to the Nyquist robust sensitivity margin proposed here, they do not provide a scalar indicator of the closeness to instability. Hence, the scalar $k_{N,s}$ can be used to compare alternative closed-loop designs and determine a hierarchy of robust stability among the alternatives. A recent result by Wang [54] concerning interval plants shows that the maximum H_∞ norm of the sensitivity function is achieved at twelve (out of sixteen) Kharitonov vertices. The result, however, applies to interval polynomials while our approach

applies to transfer functions. A systematic algorithm for the calculation of $k_{N,s}(\omega)$ is developed by taking advantage of the simple geometrical features documented in Fu [21] adopted by the Nyquist-plane images of such systems.

The chapter is organized as follows. In Section 2, the classical critical direction theory is briefly reviewed for contextual reference. Section 3 presents the definition of the new Nyquist robust sensitivity margin, discusses its properties and computational challenges, and compares and contrasts the new margin with its Nyquist robust stability margin predecessor. The application of the Nyquist robust sensitivity margin to systems with affine uncertainty structure is presented in Section 4, including the details of a systematic algorithm for the efficient calculation of the margin. Section 5 presents examples, including an illustrative case showing how to utilize the proposed method for calculating a parametric robust-stability margin that is interpreted as a blow-up factor.

2.2 Background

A general linear time invariant system (LTI) can be represented in a state space form as follows:

$$\begin{aligned} \dot{x}(t) &= Ax(t) + Bu(t) \\ y(t) &= Cx(t) + Du(t) \end{aligned} \tag{2.1}$$

Furthermore, the representation (2.1) can be expressed in the following transfer function form:

$$G(s) = C(A - sI)^{-1}B + D = C \frac{\text{adj}(sI - A)}{\det(sI - A)} B + D \tag{2.2}$$

provided there are no cancellations between the numerator and denominator polynomials. When the system matrices (A, B, C, D) are uncertain, the transfer function form is given, for the MIMO case, by $G(s) = G_0(s) + \Delta(s)$, where $G_0(s)$ is a known transfer matrix, and $\Delta(s)$ is the transfer matrix representing the uncertainty. The

transformation of system (2.1) into (2.2) allows us to use frequency domain techniques to analyze the stability and performance of the closed-loop system. Since the development of the Nyquist robust sensitivity margin in this chapter requires frequency domain techniques such as the Nyquist theorem, the transfer function form is the appropriate environment to use in assessing the robust stability of the system.

Consider the uncertain single-input/single-output transfer function

$$g(s) = g_0(s) + \delta(s) \quad (2.3)$$

shown in Figure 2.1, where $g_0(s)$ is a nominal system, $\delta(s) \in \Delta$ is an unknown perturbation belonging to a known set of allowable perturbations Δ . The closed-loop system of Figure 2.1 is said to be robustly stable if stability is ensured for all $\delta(s) \in \Delta$. The problem under consideration is the analysis of the robust stability of the uncertain closed-loop system (2.3) under negative unity feedback. The developments assume the following standard premises that are commonly used in Nyquist-based robustness analysis: (A1) the nominal transfer function $g_0(j\omega)$ is stable under negative-unity feedback, and (A2) the uncertain system $g(j\omega)$ and the nominal system $g_0(j\omega)$ have the same number of open-loop unstable poles.

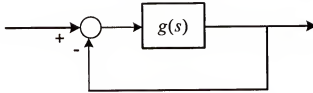


Figure 2.1: The uncertain system $g(s) = g_0(s) + \delta(s)$ in a unity-feedback configuration.

The key concepts and definitions pertaining to the critical direction theory are readily summarized utilizing Figure 2.2. First, the critical line is the oriented line (*i.e.*, a ray) in the Nyquist plane originating at the nominal point $g_0(j\omega)$ and passing through the critical point $-1 + j0$. The critical direction

$$d_c(j\omega) = -\frac{1 + g_0(j\omega)}{|1 + g_0(j\omega)|} \quad (2.4)$$

is a unit-length vector with origin at $g_0(j\omega)$ and pointing towards the critical point. Then, the critical ray is characterized by $r(\omega) = g_0(j\omega) + \alpha d_c(j\omega)$ for $\alpha \in \mathcal{R}^+$. The uncertainty value set

$$\mathcal{V}(\omega) = \{g(j\omega) : g(j\omega) = g_0(j\omega) + \delta(j\omega), \delta(s) \in \Delta\} \quad (2.5)$$

represents the Nyquist-plane mapping $g(j\omega) = g_0(j\omega) + \delta(j\omega)$ of the uncertain system. The boundary of the uncertainty value set (2.5) is denoted as $\partial\mathcal{V}(\omega)$. Finally, the *critical value set* $\mathcal{V}_c(\omega) := \mathcal{V}(\omega) \cap r(\omega)$ is the subset of $\mathcal{V}(\omega)$ that lies on the critical line.

The critical value set $\mathcal{V}_c(\omega)$ may be convex, *i.e.*, a set described as a single point or as straight-line segment (such as the straight-line segment $\overline{g_o(j\omega_i)g_s(j\omega_i)}$ joining the points $g_o(j\omega_i)$ and $g_s(j\omega_i)$ shown in Figure 2.2a), or nonconvex, *i.e.*, a union of isolated points and straight-line segments (such as the union of the disjoint segments $\overline{g_o(j\omega_i)g_1(j\omega_i)}$ and $\overline{g_2(j\omega_i)g_3(j\omega_i)}$ in Figure 2.2b). Note that it is possible to encounter an uncertain system with a highly nonconvex value set $\mathcal{V}(\omega)$ that nevertheless features a convex critical value set $\mathcal{V}_c(\omega)$, as illustrated in Figure 2.2a.

For the general case of convex or nonconvex critical value sets, Baab *et al.* [2] define the critical perturbation radius

$$\rho_c(\omega) := \begin{cases} |1 + g_0(j\omega)| - \xi(\omega) & \text{if } -1 + j0 \notin \mathcal{V}(\omega) \\ |1 + g_0(j\omega)| + \xi(\omega) & \text{otherwise} \end{cases} \quad (2.6)$$

where

$$\xi(\omega) = \min_{z \in \mathcal{B}_c(\omega)} |1 + z| \quad (2.7)$$

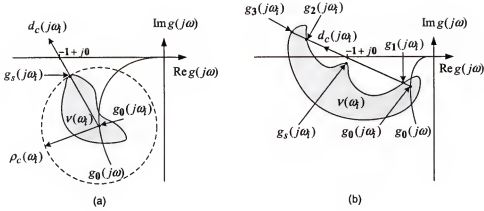


Figure 2.2: Uncertainty value sets at a frequency ω_i : (a) convex critical value set $\mathcal{V}_c(\omega_i)$, (b) nonconvex critical value set $\mathcal{V}(\omega_i)$. Both figures show the worst-sensitivity plant $g_s(j\omega_i)$, located closest to the point $-1 + j0$.

represents the minimal distance from the critical point $-1 + j0$ to the set of critical boundary intersections $\mathcal{B}_c(\omega) := \{\partial\mathcal{V}(\omega) \cap r(j\omega)\} \setminus g_0(\omega)$, where ' \setminus ' is the set-exclusion operator. In the case where $g_0(\omega)$ is the only element of $\partial\mathcal{V}(\omega) \cap r(j\omega)$, then $\mathcal{B}_c(\omega) := \{g_0(\omega)\}$. As shown in Baab et al. [2], when $\mathcal{V}_c(\omega)$ is a convex set, as illustrated in Figure 2.2a, the definition (2.6) reduces to

$$\rho_c(\omega) := \max\{\alpha \in \mathcal{R}^+ : g(j\omega) = g_0(j\omega) + \alpha d_c(j\omega) \in \mathcal{V}_c(\omega)\} \quad (2.8)$$

a form first invoked in Latchman et al. [36], where $\rho_c(\omega)$ is simply interpreted as the distance between the critical point and the point where the boundary $\partial\mathcal{V}(\omega)$ intercepts the critical direction. Finally, the Nyquist robust stability margin is defined as

$$k_N(\omega) = \frac{\rho_c(\omega)}{|1 + g_0(j\omega)|} \quad (2.9)$$

The main result of Baab et al. [2] is restated in the following theorem.

Theorem 1 *Consider the uncertain system (2.3) with assumptions (A1) and (A2). Then, the closed-loop system is robustly stable under unity feedback if and only if $k_N(\omega) < 1 \forall \omega$.*

Proof: See Baab et al. [2]. ■

Note that the theorem is valid in general for convex as well as nonconvex critical value sets $\mathcal{V}_c(\omega)$. Since control design is often carried out under sufficient-only conditions, for control synthesis purposes it may be acceptable to adopt the definition (2.8) instead of (2.6) when working with nonconvex critical value sets. Then the resulting condition $k_N(\omega) < 1 \forall \omega$, where k_N is calculated through (2.9), is only sufficient for robust stability.

2.3 The Nyquist Robust Sensitivity Margin

The main drawback of definition (2.6) is that the resulting Nyquist robust stability margin value $k_N(\omega)$ obtained through (2.6) and (2.9) may convey no information about the worst-case sensitivity in the value set. Figure 2.2b shows that at the frequency $\omega = \omega_i$ the plant $g_s(j\omega_i)$ is the element of $\mathcal{V}(\omega_i)$ that is closest to the point $-1 + j0$. Hence the sensitivity $\frac{1}{|1+g_s(j\omega_i)|}$ is the largest among all the plants in the value set. Note that since $g_s(j\omega_i) \notin \mathcal{V}_c(\omega_i)$, this plant is ignored in the classical critical direction analysis presented in Section 2 which focuses only on plants that lie along the critical direction.

In this section an alternative approach is presented to include sensitivity effects in the robustness margin. To this end we define the sensitivity perturbation radius

$$\rho_s(\omega) := \begin{cases} |1 + g_0(j\omega)| - \eta(\omega) & \text{if } -1 + j0 \notin \mathcal{V}(\omega) \\ |1 + g_0(j\omega)| + \eta(\omega) & \text{otherwise} \end{cases} \quad (2.10)$$

where

$$\eta(\omega) = \min_{z \in \partial \mathcal{V}(\omega)} |1 + z| \quad (2.11)$$

represents the minimum distance between the critical point $-1 + j0$ and the boundary set $\partial \mathcal{V}(\omega)$. Then, in a fashion analogous to (2.9), the *Nyquist robust sensitivity margin*

is defined as

$$k_{N,s}(\omega) := \frac{\rho_s(\omega)}{|1 + g_0(j\omega)|} \quad (2.12)$$

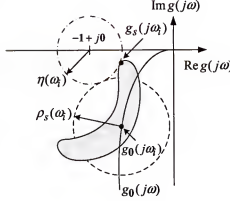


Figure 2.3: Illustration of the inverse-sensitivity circle of radius $\eta(\omega)$ introduced in definition (2.11).

Figure 2.3 gives an interpretation of $\eta(\omega)$ defined in (2.11) as the radius of the *inverse-sensitivity circle*, namely, the smallest circle with center at $-1 + j0$ that contains a point belonging to the boundary $\partial\mathcal{V}(\omega)$. Furthermore, the definition (2.11) and Figure 2.3 can be used to conclude that $\eta(\omega) = |1 + g_s(j\omega)|$, where $g_s(j\omega)$ is the perturbation in $\mathcal{V}(\omega)$ that has the worst sensitivity.

It is also of interest to note that $k_{N,s}(\omega) = 1$ corresponds to the case where $-1 + j0 \in \partial\mathcal{V}(\omega)$. This follows from the fact that $k_{N,s}(\omega) = 1$ if and only if $\eta(\omega) = 0$, and the latter equality is realized from the optimization problem (2.11) only when $-1 + j0 \in \partial\mathcal{V}(\omega)$. Finally, it is of utility for the suite to note that at all frequencies ω

$$\eta(\omega) \leq \xi(\omega) \quad (2.13)$$

This inequality is derived as follows. Since the value-set boundary $\partial\mathcal{V}(\omega)$ contains as a subset the set of critical boundary intersections $\mathcal{B}_c(\omega)$, the optimization problem (2.11) is carried out over an optimization domain that is a superset of the optimization

domain used in the optimization problem (2.7). Consequently, the solutions to the respective optimization problems must follow the relationship (2.13).

Theorem 2 *Consider the uncertain system (2.3) with assumptions (A1) and (A2). Then, the closed-loop system is robustly stable under unity feedback if and only if $k_{N,s}(\omega) < 1 \forall \omega$.*

Proof: From the zero-exclusion principle [4] it can be claimed that the uncertain system (2.3) under assumptions (A1) and (A2) is robustly stable if and only if $-1 + j0 \notin \mathcal{V}(\omega)$. Therefore, it must be shown that under the definitions (2.10)-(2.12) for $\rho_s(\omega)$, the condition $k_{N,s}(\omega) < 1$ is equivalent to the set membership condition $-1 + j0 \notin \mathcal{V}(\omega)$.

First, to prove sufficiency one must show that $k_{N,s}(\omega) < 1 \forall \omega$ implies that $-1 + j0 \notin \mathcal{V}(\omega)$. The proof proceeds by contradiction. Assume that $k_{N,s}(\omega) < 1$ and that there exists a frequency ω such that $-1 + j0 \in \mathcal{V}(\omega)$. Invoking the sensitivity-perturbation radius expression (2.10) for the case where $-1 + j0 \in \mathcal{V}(\omega)$ and the definition (2.12) it follows that

$$k_{N,s}(\omega) = \frac{\rho_s(\omega)}{|1+g_0(j\omega)|} = \frac{|1+g_0(j\omega)|+\eta(\omega)}{|1+g_0(j\omega)|} = 1 + \frac{\eta(\omega)}{|1+g_0(j\omega)|}$$

Since by definition $\eta(\omega) \geq 0$, then the equation above implies that $k_{N,s}(\omega) \geq 1$, which is a contradiction. This proves sufficiency.

Second, to prove necessity one must show that at any frequency ω the condition $-1 + j0 \notin \mathcal{V}(\omega)$ implies that $k_{N,s}(\omega) < 1$. Assume that $-1 + j0 \notin \mathcal{V}(\omega)$. Invoking the sensitivity-perturbation radius expression (2.10), now for the case where $-1 + j0 \notin \mathcal{V}(\omega)$, and the definition (2.12), it follows that

$$k_{N,s}(\omega) = \frac{\rho_s(\omega)}{|1+g_0(j\omega)|} = \frac{|1+g_0(j\omega)|-\eta(\omega)}{|1+g_0(j\omega)|} = 1 - \frac{\eta(\omega)}{|1+g_0(j\omega)|} \quad (2.14)$$

Since in this case $-1 + j0 \notin \mathcal{V}(\omega)$, it follows that $-1 + j0 \notin \partial\mathcal{V}(\omega)$, and hence from (2.11) it is concluded that $\eta(\omega) > 0$. Furthermore, from (2.11) it is obvious that

$\eta(\omega) \leq |1 + g_0(\omega)|$. Hence, it follows that $0 < \frac{\eta(\omega)}{|1 + g_0(j\omega)|} \leq 1$, which can be used in (2.14) to conclude that $k_{N,s}(\omega) < 1$. ■

Figure 2.2a illustrates a special situation where $k_{N,s}(\omega) = k_N(\omega)$. This follows from a simple argument using the elements shown in the figure, where is clear that in this case $\eta(\omega) = \xi(\omega) = |1 + g_s(j\omega)|$. Hence $\rho_s(\omega) = \rho_c(\omega)$ from (2.10) and (2.6), and therefore it follows from (2.12) and (2.9) that $k_{N,s}(\omega) = k_N(\omega)$. It is also straightforward to verify that the robustness margins satisfy the following two properties: (P1) if $k_{N,s}(\omega) < 1$, then $k_{N,s}(\omega) \geq k_N(\omega)$, and (P2) if $k_{N,s}(\omega) > 1$, then $k_{N,s}(\omega) \leq k_N(\omega)$. These two properties follow in a straightforward fashion after using the inequality (2.13), the perturbation radius definitions (2.10) and (2.6), and the robustness margin definitions (2.12) and (2.9). Although in general $k_{N,s}(\omega) \neq k_N(\omega)$, as suggested in Figure 2.2b, both margins are nevertheless equivalent as indicated in the following theorem.

Theorem 3 *The Nyquist robust sensitivity margin $k_{N,s}(\omega)$ and the Nyquist robust stability margin $k_N(\omega)$ are equivalent in the sense that (i) $k_{N,s}(\omega) < 1 \iff k_N(\omega) < 1$, (ii) $k_{N,s}(\omega) = 1 \iff k_N(\omega) = 1$, and (iii) $k_{N,s}(\omega) > 1 \iff k_N(\omega) > 1$.*

Proof: The proof of sufficiency is developed below for cases (i)-(iii). The proof of necessity for the three cases in question follows an analogous argument, and is therefore omitted here for brevity. For case (i), assume $k_{N,s}(\omega) < 1$ and utilize (2.12) to conclude that

$$\rho_s(\omega) < |1 + g_0(j\omega)| \quad (2.15)$$

Also, from Theorem 2 and from the zero-exclusion principle [4], the condition $k_{N,s}(\omega) < 1$ implies that $-1 + j0 \notin \mathcal{V}(\omega)$; hence from equations (2.6) and (2.10) the appropriate expressions for the respective perturbation radii are $\rho_c(\omega) = |1 + g_0(j\omega)| - \xi(\omega)$ and $\rho_s(\omega) = |1 + g_0(j\omega)| - \eta(\omega)$. From the latter two equations and inequality (2.13) it follows that

$$\rho_c(\omega) \leq \rho_s(\omega) \quad (2.16)$$

Inequalities (2.15) and (2.16) imply that $\rho_c(\omega) < |1 + g_0(j\omega)|$ which yields the result $k_N(\omega) < 1$ after invoking (2.9). For case (ii), assume $k_{N,s}(\omega) = 1$ and utilize (2.12) to conclude that $\rho_s(\omega) = |1 + g_0(\omega)|$, which in turn from equation (2.10) implies that $\eta(\omega) = 0$. Since $\eta(\omega) = 0$ solves the optimization problem (2.11), it follows that $-1 + j0 \in \partial\mathcal{V}(\omega)$. Now, the fact that $-1 + j0 \in \partial\mathcal{V}(\omega)$ implies that $-1 + j0 \in \mathcal{B}_c(\omega)$, where $\mathcal{B}_c(\omega)$ is the optimization domain in (2.7). Since $-1 + j0 \in \mathcal{B}_c(\omega)$, it follows that the solution to the optimization problem (2.7) is $\xi(\omega) = 0$, which can be used to conclude from (2.6) that $\rho_c(\omega) = |1 + g_0(\omega)|$. Substitution the latter equality into (2.9) yields $k_N(\omega) = 1$. For case (iii), assume $k_{N,s}(\omega) > 1$ and utilize (2.12) to conclude that

$$\rho_s(\omega) > |1 + g_0(j\omega)| \quad (2.17)$$

Also, from Theorem 2 and from the zero-exclusion principle [4], the condition $k_{N,s}(\omega) > 1$ implies that $-1 + j0 \in \mathcal{V}(\omega)$; hence from equations (2.6) and (2.10) the appropriate expressions for the respective perturbation radii are $\rho_c(\omega) = |1 + g_0(j\omega)| + \xi(\omega)$ and $\rho_s(\omega) = |1 + g_0(j\omega)| + \eta(\omega)$. From the latter two equations and inequality (2.13) it follows that

$$\rho_c(\omega) \geq \rho_s(\omega) \quad (2.18)$$

Inequalities (2.17) and (2.18) imply that $\rho_c(\omega) > |1 + g_0(j\omega)|$ which yields the result $k_N(\omega) > 1$ after invoking (2.9). ■

The Nyquist robust sensitivity margin $k_{N,s}(\omega)$ serves a role analogous to that of the structured singular value $\mu(\omega)$ [17] or the multivariable stability margin $k_m(\omega)$ [46], as a scalar indicator of robust stability. Given that the optimization problem (2.11) must be solved, the deployment of an analysis approach based on $k_{N,s}(\omega)$ requires knowledge the value-set boundary $\partial\mathcal{V}(\omega)$. Fortunately this information is available in a number of problems of interest, such as the case of systems with real affine uncertainty structure discussed in the following section.

2.4 Application to Systems with Affine Uncertainty Structure

The robust stability analysis approach proposed is applied to a class of uncertain systems with real affine uncertainty structure of the form

$$g(s, \mathbf{q}) = \frac{n_0(s) + \sum_{i=1}^p q_i n_i(s)}{d_0(s) + \sum_{i=1}^p q_i d_i(s)} \quad (2.19)$$

where $n_i(s)$ are numerator polynomials of known order ℓ and known real coefficients n_{ik} , $k = 0, 1, \dots, \ell$, $i = 0, 1, \dots, p$, and where $d_i(s)$ are denominator polynomials of known order m and known real coefficients d_{ik} , $k = 0, 1, \dots, m$, $i = 0, 1, \dots, p$. The element $\mathbf{q} \in Q$ is a vector of real perturbation parameters, where the real uncertainty domain

$$Q = \{\mathbf{q} \in \mathcal{R}^p : q_i^- \leq q_i \leq q_i^+, i = 1, 2, \dots, p\} \quad (2.20)$$

is a bounded rectangular polytope. In this case the uncertainty value set $\mathcal{V}(\omega)$ is simply the map $g(j\omega, Q) : \mathcal{R}^+ \times Q \rightarrow \mathcal{C}$.

The objective is to calculate the value of $k_{N,s}(\omega)$ as a function of frequency using the expression (2.12). This in turn requires the calculation of the sensitivity perturbation radius $\rho_s(\omega)$ through its defining equation (2.10). Note that in order to apply (2.10) two problems must be addressed, namely, the optimization program (2.11) must be solved to find the inverse-sensitivity radius $\eta(\omega)$ (*Problem I*), and the set-membership clause $-1 + j0 \notin \mathcal{V}(\omega)$ must be assessed as true or false (*Problem II*) so that the appropriate branch of equation (2.10) can be identified.

It is shown in [21] that the mapping $g(j\omega, E(Q))$ (denoted in the suite as the value-set *frame* at the frequency ω), where $E(Q)$ represents the set of edges of Q , spans the boundary set $\partial\mathcal{V}(\omega)$. Furthermore, the frame $g(j\omega, E(Q))$ is a set comprised of arcs of circles and straight-line segments [21]. More precisely, let $E_i(Q)$ and its corresponding extreme points q_i^- and q_i^+ represent the i -th edge of the rectangular polytope Q . Then the frame $g(j\omega, E(Q))$ is composed of a set of frame-elements $g(j\omega, E_i(Q))$, and each frame element is either a straight-line segment or an arc

of a circle. These simple geometric properties of the frame allow the development of a precise solution of *Problem I*. In fact, the minimization problem (2.11), which is equivalent to finding the minimum distance between the point $-1 + j0$ and the boundary of the value set, reduces to a simple geometric problem: finding the shortest distance between the point $-1 + j0$ and an arc of circle or a straight-line segment. Problem (2.11) can then be posed for each frame element, and the smallest solution found after considering all the edges of Q yields the value of $\eta(\omega)$ sought.

For completeness it is convenient to briefly summarize relevant geometrical concepts regarding lines and arcs of circles. The interested reader is referred to [15] for further details. A line passing through points $p_1, p_2 \in \mathcal{C}$ is defined by

$$L(p_1, p_2) := \{z \in \mathcal{C} : z = p_1 + u(p_2 - p_1), u \in \mathcal{R}\}$$

and a circle with radius r and center z_0 is given by

$$C(r, z_0) := \{z \in \mathcal{C} : |z - z_0|^2 = r^2\}$$

The arc $A(p_1, p_2, p_3)$ of a supporting circle $C(r, z_0)$ is described by three points.

One important issue to resolve is whether the map $g(j\omega, E_i(Q))$ of a given edge $E_i(Q)$ is a straight-line or an arc of a circle. This can be resolved by taking advantage of the *cross product*

$$p_1 \times p_2 = \begin{vmatrix} \operatorname{Re}(p_1) & \operatorname{Re}(p_2) \\ \operatorname{Im}(p_1) & \operatorname{Im}(p_2) \end{vmatrix}$$

where $|\cdot|$ represents the determinant operator. Selecting three distinct points p_1, p_2 , and p_3 of the map $g(j\omega, E_i(Q))$, it follows that if $(p_3 - p_1) \times (p_2 - p_1) < 0$ (> 0) it can be concluded that the segment is an arc of a circle turning to the right (left). If the cross product equals zero, then the three points are collinear and the segment is a straight line. Two of the points in question should be $p_1 = g(j\omega, q_i^-)$ and $p_3 = g(j\omega, q_i^+)$. The

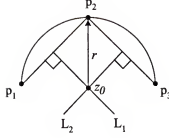


Figure 2.4: The center z_0 and radius r of the supporting circle of the arc $A(p_1, p_2, p_3)$ are determined from the intersection of the auxiliary lines L_1 and L_2

third point can be taken as the image of a distinct point on the edge $E_i(Q)$ that can be selected arbitrarily, say for example, $p_2 = g(j\omega, (q_i^- + q_i^+)/2)$.

For the case where the map $g(j\omega, E_i(Q))$ of an edge $E_i(Q)$ is an arc, the minimum distance from $-1 + j0$ to the arc can be given by either (i) the distance to one of the end points of the arc, or (ii) the distance to an internal point of the arc. Clearly, if the ray originating at the center of the supporting circle of the arc and passing through $-1 + j0$ does not intersect the arc, then the minimum distance can be determined from one of the two end points of the arc. On the other hand, if the ray intersects the arc, then the distance between $-1 + j0$ and the point of intersection defines the minimum distance sought.

Finally, the procedure described requires finding the supporting circle of an arc. From Figure 2.4, the center z_0 of the supporting circle of an arc that passes through three distinct points p_1, p_2 , and p_3 on the complex plane can be determined from the intersection of the lines $L_1 := (p_1 + p_2)/2 + ju_1(p_2 - p_1)$, and $L_2 := (p_3 + p_2)/2 + ju_2(p_3 - p_2)$, where $u_1, u_2 \in \mathcal{R}$. The radius r is then found in an obvious fashion, say for example as $r = |p_2 - z_0|$.

For the case where the map $g(j\omega, E_i(Q))$ of an edge $E_i(Q)$ is a straight-line segment, the minimum distance to the point $-1 + j0$ is found using a procedure formally similar to the case of the arcs. First a supporting line is found. Then, one finds the point of intersection between the supporting line and a normal line that

passes through $-1 + j0$. The intersection point gives the minimal distance to $-1 + j0$ if the intersection point is also an element of the straight-line segment. Otherwise, the minimum distance is defined as the distance between $-1 + j0$ and one of the two end-points of the straight-line segment.

The procedure described above solves *Problem I*, yielding a numerical value for the inverse-sensitivity radius $\eta(\omega)$ at each frequency. *Problem II* can be addressed efficiently through the assistance of the following theorem, which is a restatement of an equivalent theorem derived in Baab et al. [2]. A detailed proof is given in the original reference.

Theorem 4 *Consider the real-affine uncertain system (2.19)- (2.20) configured in the unity-feedback form given in Figure 2.3 under the assumptions (A1) and (A2). Then $-1 + j0 \notin \mathcal{V}(\omega)$ if and only if at frequency ω the following linear equality/inequality problem is infeasible:*

$$\mathbf{A}\mathbf{q} = \mathbf{b} \quad (2.21)$$

subject to

$$\mathbf{B}\mathbf{q} \leq \mathbf{b}^+ \quad (2.22)$$

where

$$\mathbf{A} := \begin{bmatrix} \mathbf{s}_{n,R}^T \mathbf{N}_{p,R} + \mathbf{s}_{d,R}^T \mathbf{D}_{p,R} \\ \mathbf{s}_{n,I}^T \mathbf{N}_{p,I} + \mathbf{s}_{d,I}^T \mathbf{D}_{p,I} \end{bmatrix} \in \mathcal{R}^{2 \times p}, \quad \mathbf{b} := \begin{bmatrix} -\mathbf{s}_{n,R}^T \mathbf{n}_{0,R} - \mathbf{s}_{d,R}^T \mathbf{d}_{0,R} \\ -\mathbf{s}_{n,I}^T \mathbf{n}_{0,I} - \mathbf{s}_{d,I}^T \mathbf{d}_{0,I} \end{bmatrix} \in \mathcal{R}^2$$

$$\mathbf{B} := \begin{bmatrix} 1 & 0 & 0 & \dots & 0 \\ -1 & 0 & 0 & \dots & 0 \\ 0 & 1 & 0 & \dots & 0 \\ 0 & -1 & 0 & \dots & 0 \\ \vdots & \vdots & \vdots & \ddots & \vdots \\ 0 & 0 & 0 & \dots & 1 \\ 0 & 0 & 0 & \dots & -1 \end{bmatrix}, \quad \mathbf{b}^+ := \begin{bmatrix} q_1^+ \\ -q_1^- \\ q_2^+ \\ -q_2^- \\ \vdots \\ q_p^+ \\ -q_p^- \end{bmatrix}$$

and

$$\mathbf{s}_{n,R}^T := [1 \ -\omega^2 \ \omega^4 \ -\omega^6 \ \dots] \in \mathcal{R}^{[l/2]+1}, \quad \mathbf{s}_{n,I}^T := [\omega \ -\omega^3 \ \omega^5 \ -\omega^7 \ \dots] \in \mathcal{R}^{[(l+1)/2]}$$

$$\mathbf{s}_{d,R}^T := [1 \ -\omega^2 \ \omega^4 \ -\omega^6 \ \dots] \in \mathcal{R}^{[m/2]+1}, \quad \mathbf{s}_{d,I}^T := [\omega \ -\omega^3 \ \omega^5 \ -\omega^7 \ \dots] \in \mathcal{R}^{[(m+1)/2]}$$

$$\mathbf{n}_{0,R} := \begin{bmatrix} n_0 \\ n_{02} \\ \vdots \end{bmatrix} \in \mathcal{R}^{[l/2]+1}, \quad \mathbf{N}_{p,R} := \begin{bmatrix} n_{10} & n_{20} & \dots & n_{p0} \\ n_{12} & n_{22} & \dots & n_{p2} \\ \vdots & \vdots & \dots & \vdots \end{bmatrix} \in \mathcal{R}^{([l/2]+1) \times p}$$

$$\mathbf{n}_{0,I} := \begin{bmatrix} n_{01} \\ n_{03} \\ \vdots \end{bmatrix} \in \mathcal{R}^{[(l+1)/2]}, \quad \mathbf{N}_{p,I} := \begin{bmatrix} n_{10} & n_{20} & \dots & n_{p0} \\ n_{12} & n_{22} & \dots & n_{p2} \\ \vdots & \vdots & \dots & \vdots \end{bmatrix} \in \mathcal{R}^{[(l+1)/2] \times p}$$

$$\mathbf{d}_{0,R} := \begin{bmatrix} d_{00} \\ d_{02} \\ \vdots \end{bmatrix} \in \mathcal{R}^{[m/2]+1}, \quad \mathbf{D}_{p,R} := \begin{bmatrix} d_{10} & d_{20} & \dots & d_{p0} \\ d_{12} & d_{22} & \dots & d_{p2} \\ \vdots & \vdots & \dots & \vdots \end{bmatrix} \in \mathcal{R}^{([m/2]+1) \times p}$$

$$\mathbf{d}_{0,I} := \begin{bmatrix} d_{01} \\ d_{03} \\ \vdots \end{bmatrix} \in \mathcal{R}^{[(m+1)/2]}, \quad \mathbf{D}_{p,I} := \begin{bmatrix} d_{11} & d_{21} & \cdots & d_{p1} \\ d_{13} & d_{23} & \cdots & d_{p3} \\ \vdots & \vdots & \cdots & \vdots \end{bmatrix} \in \mathcal{R}^{[(m+1)/2] \times p}$$

where $\lceil \cdot \rceil$ represents the greatest-integer function.

Proof: See Baab et al. [2]. ■

In summary, for the system (2.19) with parametric uncertainty (2.20) it is possible to solve *Problem I* and calculate with very high numerical precision the sensitivity radius $\eta(\omega)$ because the solution to (2.11) is given by a set of simple algebraic equations. In addition, it is possible to solve *Problem II* in a numerically efficient fashion because the condition $-1 + j0 \in \mathcal{V}(\omega)$ can be determined via a simple feasibility problem involving linear equalities and inequalities. Hence, the sensitivity perturbation radius $\rho_s(\omega)$ in (2.10) and the Nyquist robust sensitivity margin $k_{N,s}(\omega)$ in (2.12) can be computed precisely and efficiently.

2.5 Examples

Three examples are presented. The first one calculates the margins $k_{N,s}(\omega)$ and $k_N(\omega)$ to compare and contrast their values and to shed light into their interpretation. The second example illustrates in a dramatic fashion the fact that $k_{N,s}(\omega)$ provides a more meaningful indication of the degree of robust sensitivity of the closed loop. Finally, the last example is designed to illustrate how the concepts proposed here can be utilized to formulate and calculate an alternative robustness measure, namely a *parametric stability margin*.

2.5.1 Example 1

Consider the affine system of the form (2.19) with the structure [29]

$$g(s, q) = c(s) \frac{5s + q_1}{s^2 + q_2s + q_3} \quad (2.23)$$

where

$$c(s) = \frac{3603.7935 s + 18018.9673}{s^2 + 1434.5016 s - 2312.4499}$$

is a feedback controller. Let the real perturbation parameters belong to the uncertainty domain

$$Q = \{(q_1, q_2, q_3) \in \mathcal{R}^3 : 0 \leq q_1 \leq 8, -2 \leq q_2 \leq 6, -19 \leq q_3 \leq -11\} \quad (2.24)$$

Figure 2.5 shows the uncertainty value set for (2.23) at the frequency $\omega = 9$, including the corresponding sensitivity circle centered at $-1 + j0$. Note that Figure 2.5 also shows the frame of the value set of (2.23), namely, the straight-line segments and arcs of circles that result from the mapping of all the edges of Q . The problem is to analyze the robust stability of the feedback loop involving the uncertain system (2.23) subject to the uncertainty description (2.24).

The margin $k_{N,s}(\omega)$, calculated following the algorithm given in Section 4, and the margin $k_N(\omega)$, calculated using the technique described in Baab et al. [2], are plotted in Figure 2.6 for frequencies $\omega \in [10^{-3}, 10]$. Given that $k_{N,s}(\omega) < 1 \forall \omega$, it can be concluded from Theorem 2 that the closed-loop system is robustly stable. Since the two margins are equivalent, the values of $k_{N,s}(\omega) < 1$ reported in the figure correspond to values $k_N(\omega) < 1$ at the same frequency, consistent with Theorem 3. Note that Figure 2.6 shows that in this particular case $k_{N,s}(\omega)$ is

an upper observation is consistent with property (P1) which implies that $k_{N,s}(\omega)$ is an upper bound for $k_N(\omega)$ when the system is robustly stable.

2.5.2 Example 2

Consider the system [2]

$$g(s, q) = c(s) \frac{n(s)}{d(s)} \quad (2.25)$$

where $n(s) = s^2 + (4 + 0.4q_1 + 0.2q_2)s + (20 + q_1 - q_3)$, $d(s) = s^4 + (9.5 + 0.5q_1 - 0.5q_2 + 0.5q_3)s^3 + (27 + 2q_1 + q_2)s^2 + (22.5 - q_1 + q_3)s + 0.1$, $c(s) = 0.3s + 1$, and where

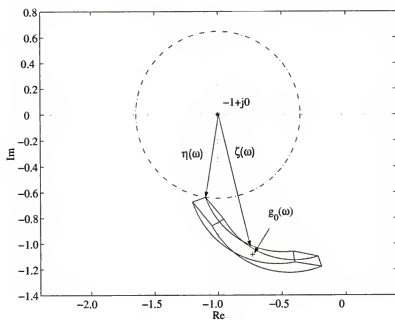


Figure 2.5: Frame for the value set of system (2.23) at $\omega = 9$, and the corresponding inverse-sensitivity circle. The nominal plant $g_0(j\omega)$ is indicated by the '+' marker.

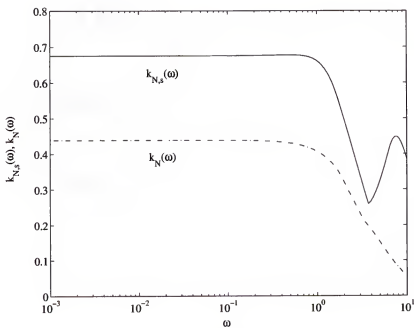


Figure 2.6: Value of $k_{N,s}(\omega)$ and $k_N(\omega)$ as a function of frequency for the first example.

the real perturbation parameters belong to the polytope

$$Q_1 = \{(q_1, q_2, q_3) \in \mathcal{R}^3 : -3 \leq q_i \leq 3, i = 1, 2, 3\} \quad (2.26)$$

Introducing a parametric blow-up factor $\alpha = 1.86$ to define a larger uncertainty domain

$$Q = \alpha Q_1 \quad (2.27)$$

such that

$$Q = \{(q_1, q_2, q_3) \in \mathcal{R}^3 : -5.58 \leq q_i \leq 5.58, i = 1, 2, 3\}$$

and using $\omega = 4.72$ yields the frame $g(j\omega, E(Q))$ depicted in Figure 2.7. The results obtained are as follows: $\rho_s(\omega) = 0.8466$, $\rho_c(\omega) = 0.0206$, $k_{N,s}(\omega) = 0.8577$, and $k_N(\omega) = 0.0209$. Both $k_{N,s}(\omega)$ and $k_N(\omega)$ are less than unity at the frequency considered. Further analysis shows that the result holds at all frequencies; hence, the closed loop system is robustly stable according to Theorem 2. Certainly, $k_{N,s}(\omega)$ and $k_N(\omega)$ are equivalent in terms of assessing the robust stability of the system, as proved in Theorem 3. However in the terms of robust performance, $k_{N,s}(\omega)$ is a more meaningful metric than $k_N(\omega)$ because the larger value of $k_{N,s}(\omega)$ better reflects the fact that the value set in Figure 2.7 is in close proximity of the critical point $-1 + j0$. In fact, at the frequency in question $k_{N,s}(\omega) = 0.8577$ is a much larger value than $k_N(\omega) = 0.0209$. The significantly smaller value of $k_N(\omega)$ does not yield comparable insight into the proximity of the worst-sensitivity perturbation to the point $-1 + j0$ because the calculation of $k_N(\omega)$ does deliberately ignores all uncertainties lying outside the critical direction.

2.5.3 Example 3

An useful application of the Nyquist robust sensitivity margin proposed is the calculation of a parametric stability margin. Consider the system (2.25) used in Example 2 and the polytope (2.26)-(2.27) featuring a variable blow-up factor $\alpha > 0$.

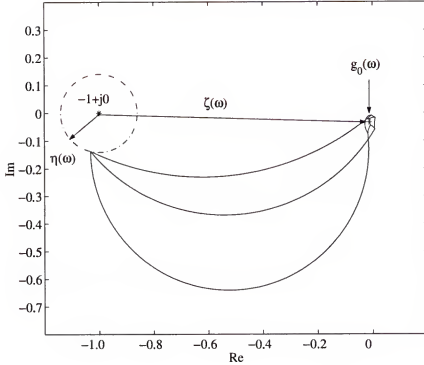


Figure 2.7: Frame for the value set of system (2.25) at $\omega = 4.72$ and $\alpha = 1.86$. The nominal plant $g_0(j\omega)$ is indicated by the '+' marker.

Figure 2.8 shows the Nyquist robust sensitivity margin $k_{N,s} := \max_{\omega} k_{N,s}(\omega)$ that results when magnifying the original perturbation polytope Q by different blow-up factor values. The numerical study shows that when the blow-up factor has the value $\alpha = 1.89$ then the Nyquist robust sensitivity margin $k_{N,s}$ is approximately equal to unity, hence reaching the limit of robust stability. The limiting value $\bar{\alpha} = 1.89$ is the *parametric robust stability margin* for the uncertain closed loop. In other words, the controller $c(s)$ introduced in Example 2 can robustly stabilize the closed-loop system subject to a parametric blow-up factor of the parametric uncertainty domain (2.27) less than $\bar{\alpha}$. Note that the blow-up factor used in Example 2 is $\alpha = 1.86 < \bar{\alpha}$; hence, the uncertain closed-loop of Example 2 is robustly stable.

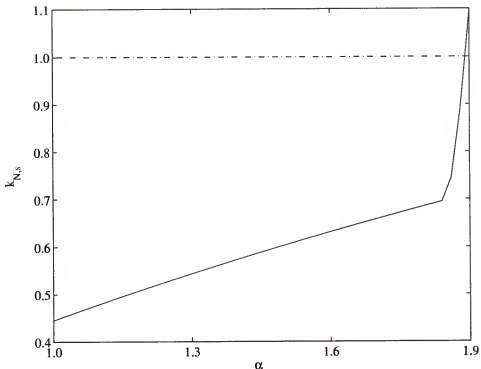


Figure 2.8: Plot of the Nyquist robust sensitivity margin $k_{N,s} = \max_{\omega} k_{N,s}(\omega)$ as a function of the blow-up factor α . The parametric robust stability margin is $\bar{\alpha} = 1.89$, which corresponds to the value of the blow-up factor α that makes $k_{N,s}$ approximately equal to unity.

2.6 Conclusions

The new concept of a Nyquist robust sensitivity margin can be used to quantify the robust stability of uncertain closed-loop systems while at the same time producing a meaningful indication of the worst-case sensitivity that is realized. Hence, in this sense the approach is more attractive than the classical Nyquist robust stability margin framework, which ignores all systems that do not lie along the critical direction, and that may therefore exclude from the analysis perturbed systems that have the worst sensitivity.

On the other hand, in general the calculation of the Nyquist robust sensitivity margin may involve more numerically intensive optimization work, since the program (2.11) is a superset of the program (2.7). In other words, the calculation of $k_{N,s}(\omega)$ requires knowledge of the entire value-set boundary $\partial\mathcal{V}(\omega)$, whereas the calculation

of $k_N(\omega)$ requires knowledge of only those points of $\partial\mathcal{V}(\omega)$ that lie along the critical direction.

The examples presented illustrate the ability of the Nyquist robust sensitivity margin methodology to produce meaningful quantitative measures of robustness for uncertain systems, even in the case where the uncertainty value set is originated by a real parametric uncertainty description. The examples also shows how the proposed paradigm can be used to characterize alternative robustness measures, such as a parametric blow-up factor for a real uncertainty description comprised of a rectangular polytope.

The numerical algorithm used to solve the problem of Section 4 calls for a modest computational requirement because the calculation of the sensitivity radius can be carried out in a straightforward fashion. It is anticipated, however, that the computational cost associated with other particular real parametric uncertainty descriptions may become significantly more expensive given that the general parametric uncertainty analysis problem is found to be NP hard [44].

2.7 Supplementary Calculation Algorithms

Further detail on the computational techniques discussed in Section 2.4 are presented in this section. First, an alternative algorithm to finding the supporting circle of an arc is introduced. Second, a simple algorithm to find the minimum distance between the critical point and a line is discussed. Finally, a technique is discussed for determining whether the intersection point of the line through the critical point and the supporting circle of the arc segment actually lies on the arc.

2.7.1 Supporting Circle of an Arc

An alternative method for finding the supporting circle on an Arc defined by three points, $A(x_1, x_2, x_3)$, is to utilize the equation of the circle. A circle that passes

through the point x and centered at the point C is given by

$$(x_r - C_r)^2 + (x_i - C_i)^2 = r^2 \quad (2.28)$$

where the subscript r refers to the real part of the complex point x , and the subscript i refers to its imaginary part. Now, using the three points that define the Arc, namely x_1, x_2 , and x_3 , into equation (2.28), the following three equations are obtained:

$$\begin{aligned} x_{r1}^2 - 2x_{r1}C_r + C_r^2 + x_{i1}^2 - 2x_{i1}C_i + C_i^2 &= r^2 \\ x_{r2}^2 - 2x_{r2}C_r + C_r^2 + x_{i2}^2 - 2x_{i2}C_i + C_i^2 &= r^2 \\ x_{r3}^2 - 2x_{r3}C_r + C_r^2 + x_{i3}^2 - 2x_{i3}C_i + C_i^2 &= r^2 \end{aligned} \quad (2.29)$$

The three equations (2.29) have three unknowns, namely C_r, C_i , and r , which precisely identify the supporting circle of the Arc defined by x_1, x_2 , and x_3 .

2.7.2 Minimum Distance between a Line and a Point

Given that uncertain systems of the form (2.19) produce either a line-segment or an Arc, it is important to be able to find the minimum distance d_{min} between the critical point $-1 + j0$ and a line-segment. The projection technique can be utilized to do just that. The following steps describe the procedure: First, given the critical point cp , and the two end-points ps and pe of the line-segment, three vectors are defined as follows:

$$v_{cp} = \begin{bmatrix} Re(cp) \\ Im(cp) \end{bmatrix} \quad v_{ps} = \begin{bmatrix} Re(ps) \\ Im(ps) \end{bmatrix} \quad v_{pe} = \begin{bmatrix} Re(pe) \\ Im(pe) \end{bmatrix}$$

Next, define the vector $v = v_{pe} - v_{ps}$, and the the direction vector $v_d = pe - ps$. Finally, the projection is computed as

$$P = \frac{(v_{cp} - v_{ps}) \cdot v}{v_d^2}$$

where the \cdot refers to the dot product operator. Now, the minimum distance is calculated based on the sign of the projection as follows:

- if $P \leq 0$ then $d_{min} = |cp - ps|$
- if $P \geq 1$ then $d_{min} = |cp - pe|$
- if $0 \leq P \leq 1$ then $d_{min} = |cp - (ps + proj(pe - ps))|$

2.7.3 Identifying Points on the Arc

One decision that has to be made in Section 2.4 is whether the intersection point of the ray originating from the center of the supporting circle of the Arc and passing through the critical point $-1 + j0$ lies on the Arc. The key step is to identify the valid Arc phase range, I_{arc} , such that if a point $p \in I_{arc}$ then p lies on the Arc. The algorithm can be summarized as follows:

- Shift the supporting circle and the intersection point p to the origin.
- Find the phase of the start and end points of the Arc, and convert them such that the phase ranges between $[0, 2\pi]$.
- Denote the smallest phase ϕ_{min} and the largest ϕ_{max} .
- Find the phase of a mid point on the Arc and denote it ϕ_m .
 - If $\phi_{min} \geq \phi_m \geq \phi_{max}$ then $I_{arc} = [\phi_{min}, \phi_{max}]$. Furthermore, if $p \in I_{arc}$ then p lies on the Arc.
 - Else if $\phi_m \leq \phi_{min}$, and $\phi_m \leq \phi_{max}$, then $I_{arc} = [0, \phi_{min}] \cup [\phi_{max}, 0]$. Thus, if $p \in I_{arc}$ then p lies on the Arc.
 - Else $I_{arc} = [\phi_{max}, \phi_m] \cup [\phi_m, 0] \cup [0, \phi_{min}]$. Therefore, if $p \in I_{arc}$ then p lies on the Arc.

CHAPTER 3

SLIDING MODE CONTROL FOR TIME-DELAY SYSTEMS

3.1 Introduction

Delay is inherit in some control systems such as processes involving heat or mass transport. The presence of delay in a dynamic system can have a destabilizing effect or can cause poor performance. Furthermore, delay can pose a significant challenge to ensure closed loop stability [27]. Throughout the literature, a variety of linear and nonlinear controllers have been used to stabilize time-delay systems, where the delay may appear in the state, input, or in both. Local and global stability conditions have also been derived to guarantee the asymptotic stability of the closed loop system.

The emphases of this work in on sliding mode control (SMC), a technique known for its robustness with respect to perturbations and system uncertainties, that has been used to stabilize systems with time delays; however, most of the literature focuses on systems with either state delay [6, 33, 43, 28] or with input delay [25, 45]. Some work has been done regarding systems with simultaneous state and input delays [22, 20, 55]. In Gouaisbaut et al. [22] a sliding mode controller is designed to stabilize a linear systems with input and state delay. The technique is based on transforming the system into a regular form [31], and then a memory control law that depends on previous values of the input is designed the ensure reaching the manifold as well as the asymptotic stability of the closed-loop system. Lyapunov-Kharsovski methods are employed to derived the stability conditions. The method presented in Feiqi et al. [20] incorporates a dynamic compensator into the switching function (manifold) in order to simplify the equivalent control law. Then, a control law that is a function of the switching manifold and the system state is utilized to stabilize a system that

features a constant delay in both a state and the input. The work by Xia et al. [55] considers the derivation of delay-independent as well as delay-dependent stability conditions for a class of linear systems with simultaneous delay in the state and the input. An integral switching function with a compensator is utilized to obtain a simple equivalent control law. The stability conditions are given in terms of LMIs.

This chapter introduces a new approach to address the problem of stabilizing a linear system featuring both state and input delay. First, a state transformation is used to map the original system into an input-delay free form where only state delays are present. Then, a new state defined as the difference between the original state and the transformed state is incorporated into the transformed system equation. Introducing an integral switching function in terms of the transformed states allows the derivation of a simple state feedback equivalent control law. This control action along with a proposed discontinuous control law are shown to drive the states to the switching manifold in finite time. Finally, using a bound on the new state, and utilizing Lyapunov techniques, the development delivers sufficient stability conditions that ensure the asymptotic stability of the closed-loop systems in terms of a constant LMI that depends on the delay of the system.

The chapter is structured as follows. In Section 3.2 the problem is formulated along with the transformation that eliminates the input delay. The design of the control law which consists of an equivalent control action and a discontinuous control action is discussed in Section 3.3. In section 3.4 the control law is shown to drive the system states to the sliding surface in finite time. Derivation of sufficient conditions for the asymptotic stability of the transformed and original systems is given in Section 3.5. A bound on the time delay tolerable by the systems is also given. The chapter concludes with an illustrative example that verifies the results in Section 3.6, and presents a summary in Section 3.7.

3.2 Problem Formulation

The time-delay system considered is of the form

$$\begin{aligned}\dot{x}(t) &= Ax(t) + A_d x(t-h) + Bu(t) + B_d u(t-h) \\ x(\tau) &= \Phi(\tau), \quad \tau \in [-h, 0] \\ u(\tau) &= \Psi(\tau), \quad \tau \in [-h, 0]\end{aligned}\tag{3.1}$$

where, $x(t) \in \mathbb{R}^n$ is the state, $u(t) \in \mathbb{R}^m$ is the control input, and A, A_d, B , and B_d are matrices of appropriate dimensions. The system delay h is considered to be constant, $\Phi(\tau)$ is an initial-state function, and $\Psi(\tau)$ is an initial-input function. The notation $|\cdot|$ is used to indicate, dependent on the scalar or vector nature of the argument, an absolute value of a scalar quantity or a vector norm, and $\|\cdot\|$ is used to indicate an induced matrix norm.

System Transformation. The following state transformation is introduced as suggested in [1] to map (3.1) into an input-delay free system:

$$z(t) = x(t) + \int_{t-h}^t e^{A(t-h-\tau)} B_d u(\tau) d\tau\tag{3.2}$$

Differentiating equation (3.2) to obtain

$$\dot{z}(t) = \dot{x}(t) + A \int_{t-h}^t e^{A(t-h-\tau)} B_d u(\tau) d\tau + e^{-Ah} B_d u(t) - B_d u(t-h)$$

and then substituting for $\dot{x}(t)$ from (3.1) gives

$$\dot{z}(t) = Az(t) + A_d x(t-h) + \bar{B}u(t)$$

where $\bar{B} = B + e^{-Ah} B_d$. In this work it is assumed that the pair (A, \bar{B}) is controllable.

Let's define the new state

$$v(t) := \int_{t-h}^t e^{A(t-h-\tau)} B_d u(\tau) d\tau\tag{3.3}$$

Then, the transformed system becomes

$$\dot{z}(t) = Az(t) + A_d z(t-h) + \bar{B}u(t) + \hat{A}_d v(t-h) \quad (3.4)$$

where $\hat{A}_d = -A_d$. Note that from (3.2), $v(t) = z(t) - x(t)$ is interpreted as the difference between the original system $x(t)$ and the transformed system $z(t)$. A feedback matrix F is introduced such that $\bar{A} = A - \bar{B}F$ is Hurwitz [47]. Treating the last term in (3.4) as an internal disturbance and defining $f(t, v(t-h)) := \hat{A}_d v(t-h)$, the system equation (3.4) can be rewritten as

$$\dot{z}(t) = (\bar{A} + \bar{B}F)z(t) + A_d z(t-h) + \bar{B}u(t) + f(t, v(t-h)) \quad (3.5)$$

which is free from input delay.

3.3 Switching Function and Control Law Design

The first step in the design of a sliding mode controller is to define a switching function (manifold) along which the system possesses desired properties, such as stability. Various structures of the switching functions have been used in the SMC literature. The most common designs used, however, are the basic form $s(t) = Cx(t)$, the integral form [47], and the dynamic or compensated form [55]. The basic form is best suited for systems having the general structure $\dot{x}(t) = Ax(t) + Bu(t)$. The Integral form, adopted in our work, has the advantage of cancelling the delay terms, which allows obtaining a simple state-feedback equivalent control law as is shown later. The dynamic form is preferred when known disturbances and/or delays exist in the system, as it helps to cancel these terms hence yielding a simple equivalent-control law.

The sliding surface is defined by a scalar switching function $s(t) \in \Re$ of the integral form

$$s(t) = Cz(t) - \int_0^t [C\bar{A}z(\tau) + CA_d z(\tau-h)] d\tau \quad (3.6)$$

where C is a design matrix chosen such that $C\bar{B}$ is nonsingular. The structure of the control law is given by

$$u(t) = u_e(t) + u_d(t) \quad (3.7)$$

where $u_e(t)$ is the equivalent part and $u_d(t)$ is the discontinuous part of the control law. The equivalent control is obtained by setting to zero the derivative of equation (3.6) with respect to time, and then solving for $u(t)$ to yield

$$\dot{s}(t) = C\dot{z}(t) - C\bar{A}z(t) - CA_dz(t-h) = 0$$

Following the standard approach in SMC, the state derivative $\dot{z}(t)$ in the above equation is taken from (3.5) after ignoring the disturbance term $f(t, v(t-h))$. This gives the identity

$$C(\bar{A} + \bar{B}F)z(t) + CA_dz(t-h) + C\bar{B}u(t) - C\bar{A}z(t) - CA_dz(t-h) = 0$$

which reduces to

$$C\bar{B}Fz(t) + C\bar{B}u(t) = 0$$

The solution to the above identity is $u(t) = u_e(t)$; hence, after recognizing that $C\bar{B}$ is invertible it is possible to conclude that the equivalent control law sought is

$$u_e(t) = -Fz(t) \quad (3.8)$$

The discontinuous control law proposed is

$$u_d(t) = -(C\bar{B})^{-1}[ks(t) + \rho(t) \operatorname{sgn}(s(t))] \quad (3.9)$$

where

$$\rho(t) = \|C\| \|\hat{A}_d\| |v(t-h)| + \zeta \quad (3.10)$$

and where $k > 0$ and $\zeta > 0$ are design parameters, and $v(t-h) = z(t-h) - x(t-h)$. It must be noted that the discontinuous part is what matters; however, the linear term in equation (3.9) (*i.e.*, $ks(t)$) helps smooth out the trajectories. Various structures of the discontinuous control law can be found in Hung et al. [26].

3.4 Existence of a Sliding Mode

By "Existence of a sliding mode" we mean that the system trajectories must be forced to reach the sliding surface in finite time and stay there forever. Defining a Lyapunov function $V(t) = \frac{1}{2}s^T(t)s(t)$, then in order to assure reaching the manifold in finite time it suffice to show that $\dot{V}(t) < 0$. The following Theorem provides the proof.

Theorem 1 *The time-delay system (3.5) with control law (3.7)-(3.10) reaches the sliding manifold within a finite time t_s , where*

$$t_s = \frac{1}{k} \ln \left(1 + \frac{k |s(0)|}{\zeta} \right) \quad (3.11)$$

Proof: Select $V(t) = \frac{1}{2}s(t)^2$ as a candidate scalar Lyapunov function. Then,

$$\begin{aligned} \dot{V}(t) &= s(t)\dot{s}(t) = s(t)(C\dot{z}(t) - C\bar{A}z(t) - CA_dz(t-h)) \\ &= s(t)\{C(\bar{A} + \bar{B}F)z(t) + CA_dz(t-h) \\ &\quad + C\bar{B}[-Fz(t) - (C\bar{B})^{-1}(ks(t) + \rho(t) \operatorname{sgn}(s))]\} \\ &\quad + Cf(t, v(t-h)) - C\bar{A}z(t) - CA_dz(t-h) \} \\ &= s(t)(-ks(t) - \rho(t) \operatorname{sgn}(s)) + Cf(t, v(t-h)) \\ &= -k|s(t)|^2 - \rho(t)|s(t)| + Cf(t, v(t-h))s(t) \end{aligned}$$

Now, since $|Cf(t, v(t-h))| \leq \|C\| \|\hat{A}_d\| |v(t-h)|$, after invoking (3.10) it follows that

$$\dot{V}(t) \leq -k|s(t)|^2 - \zeta|s(t)| \quad (3.12)$$

Therefore, $\dot{V}(t) < 0$ for all $k > 0$ and $\zeta > 0$, and it can be concluded that the system trajectories attain sliding mode in finite time. An estimate for the upper bound of the reaching time t_s can be obtained by integrating the differential equation $\dot{V}(t) = -k|s(t)|^2 - \zeta|s(t)|$, where $|s(t)| = \sqrt{2V(t)}$, under the initial condition $V(0) = \frac{1}{2}s(0)^2$. The result (3.11) is obtained after a simple transformation of variables and a simple algebraic manipulations. The derivation of

the reaching time for the cases $k = 0$ and $k \neq 0$ is presented in Appendix A.

■

3.5 System Stability

After demonstrating reaching the sliding manifold in finite time, it remains to show that once the system trajectories are in the sliding phase the system is asymptotically stable. At sliding mode the control law (3.7) reduces to $u(t) = u_e(t)$. Then, from (3.8) it follows that the dynamic system (3.5) is given by the expression

$$\dot{z}(t) = \bar{A}z(t) + A_d z(t-h) + f(t, v(t-h)) \quad (3.13)$$

The developments in the suite make use of the inequality

$$|v(t)| \leq \eta(h) |z(t)| \quad (3.14)$$

where

$$\eta(h) = h \max_{0 \leq \theta \leq h} \|e^{-A\theta}\| \|B_d\| \|F\| \alpha \quad (3.15)$$

and where $\alpha > 1$ is a constant derived using a Razumikhin-like argument. The purpose of this constant is to describe the evolution of $|z(t)|$, i.e., $|z(\theta)| \leq \alpha |z(t)|$, $\theta \in [t-h, t]$. The bound (3.14) follows from applying successive bounding operations to the right-hand side of (3.3) and introducing the Razumikhin parameter. The complete derivation of the constant bound in (3.15) is given in Appendix B.

We are ready now to provide the sufficient conditions for the asymptotic stability of the system (3.13) which are introduced by the following theorem.

Theorem 2 *The time delay system (3.5) with control law (3.7)-(3.10) is asymptotically stable at sliding mode if there exist positive-definite matrices $P \in \mathbb{R}^{n \times n}$, $R \in \mathbb{R}^{n \times n}$, and $Q \in \mathbb{R}^{n \times n}$ such that*

$$\lambda_{\min}(R) > \lambda_{\max}(Q) \quad (3.16)$$

and

$$\lambda_{\min}(Q)(\lambda_{\min}(R) - \lambda_{\max}(Q)) > (1 + \eta(h))^2 \|PA_d\|^2 \quad (3.17)$$

where P and R are solutions to the Lyapunov equation

$$P\bar{A} + \bar{A}^T P = -R \quad (3.18)$$

Proof: Consider a Lyapunov functional of the form

$$V(t) = z^T(t)Pz(t) + \int_{t-h}^t z^T(\tau)Qz(\tau)d\tau \quad (3.19)$$

The time derivative of $V(t)$ with respect to time is given by

$$\dot{V}(t) = 2z^T(t)P\dot{z}(t) + (z^T(t)Qz(t) - z^T(t-h)Qz(t-h))$$

Substituting the expression for $\dot{z}(t)$ given in (3.13) yields

$$\begin{aligned} \dot{V}(t) &= 2z^T(t)P\bar{A}z(t) + 2z^T(t)PA_dz(t-h) \\ &\quad + 2z^T(t)Pf(t, v(t-h)) + z^T(t)Qz(t) \\ &\quad - z^T(t-h)Qz(t-h) \end{aligned} \quad (3.20)$$

and then using (3.18) and bounding the right-hand side of (3.20) yields

$$\begin{aligned} \dot{V}(t) &\leq -\lambda_{\min}(R)|z(t)|^2 + \lambda_{\max}(Q)|z(t)|^2 \\ &\quad + 2\|PA_d\||z(t)||z(t-h)| \\ &\quad + 2\|P\hat{A}_d\||z(t)||v(t-h)| - \lambda_{\min}(Q)|z(t-h)|^2 \end{aligned} \quad (3.21)$$

Invoking the bound (3.14) and rearranging terms, inequality (3.21) can be written in the form

$$\dot{V}(t) \leq \begin{bmatrix} z(t)^T \\ z(t-h)^T \end{bmatrix}^T \begin{bmatrix} a & b \\ c & d \end{bmatrix} \begin{bmatrix} z(t) \\ z(t-h) \end{bmatrix} \quad (3.22)$$

where

$$\begin{bmatrix} a & b \\ c & d \end{bmatrix} := \begin{bmatrix} \lambda_{\max}(Q) - \lambda_{\min}(R) & (1 + \eta(h)) \|PA_d\| \\ (1 + \eta(h)) \|PA_d\| & -\lambda_{\min}(Q) \end{bmatrix} \quad (3.23)$$

To prove asymptotic stability, the Lyapunov functional must satisfy $\dot{V}(t) < 0$ which implies that the matrix (3.23) must be negative-definite. This is ensured if and only if conditions (3.16) and (3.17) are satisfied. ■

Theorem 2 can be reformulated to show explicitly the constraint on the size of the delay parameter imposed by design choices, such as the adopted Lyapunov matrices R and Q . This is given in the following corollary.

Corollary 1 *The time-delay system (3.5) with control law (3.7)-(3.10) is asymptotically stable in sliding mode for time-delay values satisfying*

$$h \max_{0 \leq \theta \leq h} \|e^{-A\theta}\| \leq \left(\frac{1}{2} \frac{\lambda_{\min}(R)}{\|PA_d\|} - 1 \right) \frac{1}{\|B_d\| \|F\| \alpha} \quad (3.24)$$

where P and R are positive-definite solutions to the Lyapunov equation (3.18) and satisfy the inequality

$$\lambda_{\min}(R) > \max(\lambda_{\max}(Q), 2\|PA_d\|) \quad (3.25)$$

Proof: The proof consists of deriving conditions that ensure the existence of a feasible solution to (3.16) and (3.17). The proof also recognizes that $\lambda_{\max}(Q)$ represents the maximum eigenvalue to the Lyapunov functional (3.19), hence $\lambda_{\min}(Q) \leq \lambda_{\max}(Q)$. Using the latter inequality along with the constraint imposed on $\lambda_{\min}(Q)$ by (3.17), it follows that

$$\frac{(1 + \eta(h))^2 \|PA_d\|^2}{\lambda_{\min}(R) - \lambda_{\max}(Q)} < \lambda_{\min}(Q) \leq \lambda_{\max}(Q) \quad (3.26)$$

A solution $\lambda_{\min}(Q)$ to (3.26) exists only if

$$\frac{(1 + \eta(h))^2 \|PA_d\|^2}{\lambda_{\min}(R) - \lambda_{\max}(Q)} < \lambda_{\max}(Q) \quad (3.27)$$

which, using the fact that (3.16) requires that $\lambda_{\min}(R) - \lambda_{\max}(Q) > 0$, is equivalent to

$$\lambda_{\max}(Q)^2 - \lambda_{\min}(R)\lambda_{\max}(Q) + (1 + \eta(h))^2 \|PA_d\|^2 < 0 \quad (3.28)$$

The analysis of the above inequality reduces to investigating the boundary defined by the equality

$$\lambda_{\max}(Q)^2 - \lambda_{\min}(R)\lambda_{\max}(Q) + (1 + \eta(h))^2 \|PA_d\|^2 = 0 \quad (3.29)$$

which can be readily solved to yield

$$\lambda_{\max}(Q) = \frac{\lambda_{\min}(R)}{2} + \frac{1}{2} \sqrt{\lambda_{\min}(R)^2 - 4(1 + \eta(h))^2 \|PA_d\|^2}$$

Given that only real solutions are meaningful, it follows that the discriminant must be nonnegative, *i.e.*,

$$\lambda_{\min}(R) \geq 2(1 + \eta(h)) \|PA_d\| \quad (3.30)$$

The presence of the factor $(1 + \eta(h)) > 1$ implies that a feasible solution to (3.30) exists only if

$$\lambda_{\min}(R) > 2 \|PA_d\| \quad (3.31)$$

Furthermore, from (3.30) it follows that the set of feasible solutions is given by the equivalent inequality

$$\eta(h) \leq \frac{1}{2} \frac{\lambda_{\min}(R)}{\|PA_d\|} - 1$$

which establishes condition (3.24) of the corollary after using (3.15) and suitably rearranging the factors in the inequality. Moreover, since $\lambda_{\min}(R)$ must simultaneously satisfy condition (3.16) and constraint (3.31), it follows that it must satisfy condition (3.25) of the corollary. ■

It remains to show the asymptotic stability of system (3.1), as addressed in the following theorem.

Theorem 3 *The time-delay system (3.1) with state $x(t)$ is asymptotically stable if the transformed system (3.5) reaches the sliding manifold and is asymptotically stable on the manifold.*

Proof: If $z(t)$ reaches the sliding surface, then the control law reduces to $u(t) = -Fz(t)$, and (3.2) can be rearranged in the form

$$x(t) = z(t) + \int_{t-h}^t e^{A(t-h-\tau)} B_d F z(\tau) d\tau \quad (3.32)$$

Now when (3.5) is asymptotically stable, it follows that $z(t) \rightarrow 0$, then $x(t) \rightarrow 0$ in (3.32), hence completing the proof. ■

The ensuing discussion presents an example that illustrates the results. From Figure (3.1), the chattering phenomenon in the control action is obvious. Chattering refers to high-frequency finite-amplitude signals. It is mainly due to the discontinuous control law. Chattering is undesirable because it can excite neglected high-frequency components, and lead to premature wear of the actuators.

Several approaches have been proposed in the literature to alleviate or eliminate the effect of chattering. Slotine [49] [50] proposed the use of a boundary layer such that standard SMC is used outside the boundary, and an approximated version of it takes affect inside the boundary. The work of Bartolini [5] introduces a new scheme to chattering reduction. The system order is increased and an estimator based on the augmented plant is defined. Also, a suitable manifold is defined such that the derivative of the control law is discontinuous on this manifold. Finally, this control law is feed through an integrator placed in the plant to yield a continuous control law. In [34], the actuator dynamics are treated as un-modelled dynamics, and thus are not part of the control law. Instead, the pass filter characteristics of the actuators are utilized to smooth out the chattering introduced by the discontinuous control action.

3.6 Example

Consider the time-delay system (3.1) with $h = 0.8$, with an initial-input function $\Psi(\tau) = 0$ for $\tau \in [-h, 0)$, and an initial-state function $\Phi(\tau) = [-1 \ 2]^T$ for $\tau \in [-h, 0]$ so that the initial-state vector is $x(0) = [-1 \ 2]^T$, and the following system parameters:

$$A = \begin{bmatrix} -1 & 0 \\ 0.2 & 0.3 \end{bmatrix}, \quad A_d = \begin{bmatrix} 0.01 & -0.04 \\ 0.02 & 0 \end{bmatrix}, \quad B = \begin{bmatrix} 2 \\ 1 \end{bmatrix}, \quad B_d = \begin{bmatrix} 1 \\ 0 \end{bmatrix}$$

The control design considered is based on the following matrices associated with the Lyapunov equation (3.18) and the Lyapunov functional (3.19):

$$R = \begin{bmatrix} 6 & 0 \\ 0 & 6 \end{bmatrix}, \quad Q = \begin{bmatrix} 3 & 0 \\ 0 & 3 \end{bmatrix}, \quad P = \begin{bmatrix} 4.5435 & 5.7537 \\ 5.7537 & 48.4578 \end{bmatrix}$$

Using the feedback matrix $F = [-0.0166 \ 0.2827]$ the eigenvalues of \bar{A} are placed at $\{-0.4, -0.45\}$. The controller parameters are $k = 30$ and $\zeta = 3$. The switching function's initial value is $s(0) = 3$, and its design matrix is chosen as $C = [0.9 \ 0.85]$. Selecting $\alpha = 2.3391$, calculating the norms of $\|B_d\| = 1$, $\|F\| = 0.2832$, and evaluating $\max_{0 \leq \theta \leq h} \|e^{-A\theta}\| = 2.2381$, then equation (3.15) gives $\eta(h) = 1.1858$. It is now straightforward to verify that conditions (3.16) and (3.17) of Theorem 2 are satisfied. First, condition (3.16) is met given that $\lambda_{\min}(R) = 6$ is greater than $\lambda_{\max}(Q) = 3$. Also, condition (3.17) is met since $\lambda_{\min}(Q)(\lambda_{\min}(R) - \lambda_{\max}(Q)) = 9$ is greater than $(1 + \eta(h))^2 \|PA_d\|^2 = 5.4770$. It follows then that Theorem 2 ensures the asymptotic stability of the closed loop system. The conditions of Corollary 1 are also satisfied since this corollary is equivalent to Theorem 2. In fact, $h \max_{0 \leq \theta \leq h} \|e^{-A\theta}\| = 1.7905$ is less than $(\frac{1}{2} \frac{\lambda_{\min}(R)}{\|PA_d\|} - 1) \frac{1}{\|B_d\| \|F\| \alpha} = 2.7208$, and $\lambda_{\min}(R) = 6$ is greater than $\max(\lambda_{\max}(Q), 2\|PA_d\|) = 3$.

Figure 3.1 shows the results of a simulation study. Figure 3.1(a) depicts the asymptotic stability of the transformed system (3.5) with state variable $z(t)$. The state trajectories for the original system (3.1) with state variable $x(t)$ are shown in Figure 3.1(b). Equation (3.11) yields $t_s = 0.1145$, a value that is consistent with the time at which $s(t)$ becomes identically zero in Figure 3.1(d), given that at that instant $z(t)$ has reached the sliding manifold. It is apparent that the states $x(t)$ develop asymptotic behavior after a time $t \approx t_s + h = 0.9145$, which is a consequence of the fact that the original system has an input delay whereas the transformed system is free of input delay. Figure 3.1(c) shows the control action $u(t)$ rising quickly from its initial value, and reaching the value of zero at approximately the same time that $z(t)$ reaches the sliding manifold. Figure 3.1(c) also shows that the control scheme suffers from a chattering effect, as is to be expected from the presence of the *signum* function in the discontinuous control law (3.9).

The chattering of the signal can be alleviated by introducing the approximation

$$\text{sgn}(s) \approx \frac{s}{|s| + \epsilon}$$

Figure 3.2 shows that a value of $\epsilon = 0.001$ effectively makes the chattering disappear (see Figure 3.2(c)), while the state trajectories $z(t)$, $x(t)$, and the switching function $s(t)$ remain virtually unchanged.

Remark 1 *The negative definiteness of the constant matrix (3.23) can be checked directly through the Linear Matrix Inequality (LMI) toolbox of Matlab.*

3.7 Conclusions

A sliding mode controller has been designed to stabilize a linear system with state and input delay. A key step is the use of a transformation to map the system input-delay free. This transformation is also used to define a new state appears as

a disturbance in the transformed system. A SMC is then designed to stabilize the state-delay system. The controller is shown to successfully drive the system states to the sliding surface in finite time. Sufficient stability conditions are derived using Lyapunov techniques.

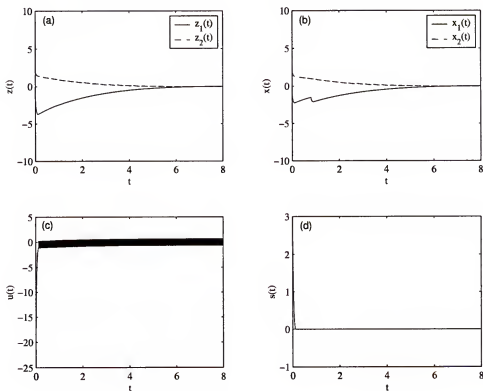


Figure 3.1: Trajectories for the states of the transformed system (a), the states of the original system (b), the control law (c), and the switching function (d).

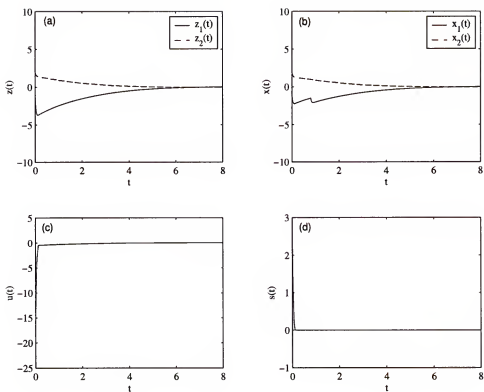


Figure 3.2: Trajectories for the states of the transformed system (a), the states of the original system (b), the control law (c), and the switching function with approximation to the signum function (d).

CHAPTER 4

STATE FEEDBACK CONTROL OF TIME-DELAY BILINEAR SYSTEMS

4.1 Introduction

This chapter considers the stabilization of a class of state-delayed bilinear system with constant delay. Much work has been done to derive sufficient conditions for the asymptotic stability of the closed-loop bilinear systems via a variety of controllers, including state feedback [24], quadratic feedback [11], and nonlinear control [10, 12]. Work has also been done to derive stability conditions for time-delay bilinear systems. The combination, however, of the time-delay and the nonlinearity makes the design of stabilizing controllers as well as the analysis much more challenging. Stability conditions can be either delay-independent or delay-dependent. Delay-independent conditions do not give any information regarding the size of the delay tolerable by the system and therefore they are generally more conservative. On the other hand, delay-dependent conditions provide information about the bound of the delay, which leads to less conservatism [18]. The former provide no information about the delay tolerable by the system. Some results can be found in [13, 23, 24, 42]. In Chiang [13], the stability analysis of a class of input-delay bilinear systems is considered. The derivations utilize the Razumikhin parameter in conjunction with matrix measure techniques [52]. The stabilization of a class of state-delay bilinear systems with saturating actuators is investigated in Niculescu et al. [42]. The work by Ho et al. [24] utilizes a memory state-feedback control law to yield global stability conditions for a class of time-delay bilinear systems. In Guojun [23], the stabilization of a class of time-varying bilinear systems with output-feedback is studied. Delay-dependent conditions are given in Liu [37], where a memoryless state-feedback control law is

used to derive stability conditions for a time-delay bilinear system with saturating actuators.

In this chapter, the stability analysis of a class of state-delay bilinear systems via state feedback control is investigated. Lemmas 2 and 3 are developed to facilitate the proof of the main theorem. The analysis utilizes the matrix measure [52], and a technique that allow expressing the stability conditions in terms of a bound on the system delay and an initial condition region of attraction. As a result, delay-dependent stability conditions are derived.

The chapter is organized as follows. Section 4.2 presents the problem along with a controllability assumptions. Section 4.3 of the paper introduces preliminary results which will be utilized in the proof of the main result. The main result is presented in Section 4.4, followed by an example and conclusions in Sections 4.5 and 4.6, respectively.

4.2 Problem Statement

Consider the system

$$\begin{aligned}\dot{x}(t) &= Ax(t) + A_d x(t-h) + Bu(t) + Nx(t)u(t) \\ x(\phi) &= \Psi(\phi), \phi \in [-h, 0]\end{aligned}\tag{4.1}$$

where $t \in \Re$ is the time variable, $x(t) \in \Re^n$ is the state, $u(t) \in \Re$ is a scalar input, A, A_d, N , and B are matrices of appropriate dimensions, and $\Psi(\phi)$ is an initial-state function. The non-negative system delay h is considered to be constant. In our development, the following conventions are used: the notation $|\cdot|$ is used to denote a vector p -norm, and the notation $\|\cdot\|$ is used to denote the induced matrix p -norm. Finally, $\mu(\cdot)$ is used to denote the matrix-measure function (see Appendix E for definition and useful properties) based on the induced matrix p -norm. Also, the following two assumptions are adopted:

(A1) the pair (A, B) is controllable.

(A2) the pair $(A + A_d, B)$ is controllable.

Our objective is to find a linear state feedback control of the form

$$u(t) = Fx(t) \quad (4.2)$$

that renders the closed-loop system asymptotically stable. We also aim at deriving delay-dependent stability conditions which guarantee the asymptotic stability of the system for initial conditions lying in a specified region, the region of attraction. Under the feedback control (4.2) the closed-loop system becomes

$$\dot{x}(t) = \bar{A}x(t) + A_dx(t-h) + Nx(t)Fx(t) \quad (4.3)$$

where $\bar{A} = A + BF$ is Hurwitz stable.

4.3 Preliminary Results

The main stability results are given in Theorem 1 for the proof of which use is made of the following three lemmas.

Lemma 1 *Consider the scalar differential equation*

$$\dot{y}(t) = ay(t)^2 + by(t) \quad (4.4)$$

where $a > 0$, and $b \neq 0$. Then the analytic solution is given by [13]

$$y(t) = \frac{be^{bt} y(0)}{b + a y(0) (1 - e^{bt})} \quad (4.5)$$

where $y(0)$ is the initial condition.

Proof: The derivation of the analytic solution (4.5) is given in Appendix C. Furthermore, a thorough discussion of the solution behavior is provided in Section 4.7

along with a graphical interpretation of the solution. Now, the finite escape time, t_f , for which $y(t_f) \rightarrow \infty$ can be found by setting the denominator of (4.5) to zero. In our development, the focus is on non-negative initial conditions, $y(0) > 0$ that are not equilibrium points of (4.4) (i.e., $y(0) \neq 0$ and $y(0) \neq -\frac{b}{a}$). If $0 < y(0) < -\frac{b}{a}$ and $b < 0$, then there is no finite escape time, and from (4.5) the following observations are readily verified:

$$(i) \quad y(t) > 0 \quad \forall t < \infty$$

$$(ii) \quad y(t+T) < y(t) \quad \forall t < T < \infty$$

$$(iii) \quad \lim_{t \rightarrow \infty} y(t) = 0 \quad \blacksquare$$

Remark 1 *It should be noted that Claims (i) and (iii) can be verified from the analytical solution (4.5). The proof of Claim (i) is given in Appendix D. Claim (ii) can be proved by verifying that (4.5) implies the inequality $y(t+T) < y(t) \quad \forall t < T < \infty$. The complete proof is given in Appendix D.*

Lemma 2 *Consider the scalar differential equation*

$$\dot{z}(t) = az(t)^2 + bz(t) + c_0 \quad (4.6)$$

where $a > 0$, $b < 0$, and $c_0 > 0$. Let k_1 and k_2 be the roots of $az(t)^2 + bz(t) + c_0$. If $b^2 > 4ac_0$, and $k_1 < z(0) < k_2$, then

$$(i) \quad z(t) > 0 \quad \forall t < \infty$$

$$(ii) \quad z(t+T) < z(t) \quad \forall t < T < \infty$$

$$(iii) \quad z(t) \rightarrow k_1 \text{ as } t \rightarrow \infty$$

Proof: The condition $b^2 > 4ac_0$ implies that k_1 and k_2 are real distinct roots. Introducing the state transformation

$$y(t) = z(t) + r \quad (4.7)$$

where r is a real constant to be determined, and combining the time derivative of (4.7) with equation (4.6) yields

$$\dot{y}(t) = a y(t)^2 + (b - 2ar)y(t) + ar^2 - br + c_0 \quad (4.8)$$

The quadratic form defined by the last three terms on the right-hand side of equation (4.8) is set to zero by the values

$$r_1, r_2 = \frac{b \mp \sqrt{b^2 - 4ac_0}}{2a} \quad (4.9)$$

where $r_1 < r_2$. One can easily verify that $k_1 = -r_2 > 0$ and $k_2 = -r_1 > 0$. The objective is to select a value of r that renders the coefficient $b - 2ar < 0$ in equation (4.8). This is realized if and only if $\frac{b}{2a} < r$, which as a consequence of equation (4.9) is satisfied by selecting $r = r_2$, where r_2 is the largest root. Therefore, substituting $r = r_2$ into equation (4.8) yields

$$\dot{y}(t) = a y(t)^2 + (b - 2ar_2)y(t) \quad (4.10)$$

Now, equation (4.10) has the same form as equation (4.4); hence, Lemma 1 can be applied to conclude that $y(t) \rightarrow 0$ as $t \rightarrow \infty$, provided that $0 < y(0) < -\frac{b-2ar_2}{a}$. From the transformation equation (4.7), it follows that $z(t) \rightarrow -r_2 = k_1$ as $t \rightarrow \infty$, provided that the initial condition satisfies $z(0) < -\frac{b+ak_1}{a} = k_2$. This proves claim (iii) of the lemma. Claims (i) and (ii) can be readily verified from Lemma 1 and the transformation (4.7). First, since $y(t) > 0$ then $z(t) > -r_2 > 0$. Second, since $y(t)$ is strictly monotonically decreasing it follows that its shifted version $z(t)$ is also strictly monotonically decreasing. ■

Remark 2 The arrows on the z -axis of Figure 4.1a show that the solution converges to the smaller equilibrium point k_1 whenever the initial condition satisfies $z(0) < k_2$. Figure 4.1b shows the conceptual state trajectories for three different initial conditions.

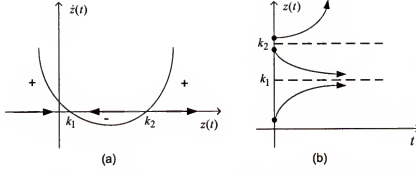


Figure 4.1: Graphical interpretation of the differential equation of Lemma 2: (a) derivative graph, (b) solution curves

Lemma 3 Consider the scalar system

$$\dot{z}(t) = az(t)^2 + bz(t) + hc_1 \sup_{t-2h \leq \theta \leq t} z(\theta) + hc_2 \sup_{t-2h \leq \theta \leq t} z(\theta)^2 \quad (4.11)$$

where $h > 0$, $a > 0$, $c_1 > 0$, $c_2 > 0$, $b < 0$, and where the initial-state function

$$\psi(\phi) = z(\phi) > 0, \quad \phi \in [-2h, 0] \quad (4.12)$$

satisfies $\sup_{-2h \leq \theta \leq 0} z(\theta) = z(0)$. If

$$\frac{-b - \sqrt{b^2 - 4ac_0}}{2a} < z(0) < \min\left\{-\frac{b + hc_1}{a + hc_2}, \frac{-b + \sqrt{b^2 - 4ac_0}}{2a}\right\} \quad (4.13)$$

and

$$h < \min\left\{\frac{b^2}{4a\bar{c}_0}, -\frac{b}{c_1}\right\} \quad (4.14)$$

where $c_0 = h(c_1 z(0) + c_2 z(0)^2)$, and $\bar{c}_0 = \frac{c_0}{h}$, then

- (i) $z(t) > 0 \quad \forall t < \infty$
- (ii) $z(t+T) < z(t) \quad \forall t < T < \infty$
- (iii) $\lim_{t \rightarrow \infty} z(t) = 0$

Proof: Let $\tau = 2h$. Now, consider an initial condition that satisfies (4.13), hence $z(0) > 0$, and assume that at some time $t_2 < \infty$ the state function satisfies $z(t_2) < 0$,

and that the state changes sign for the first time at an instant $t_1 < t_2$ such that $t_2 - t_1 < \tau$. This scenario can hold only if $\dot{z}(t) < 0$ at some time $t \in (t_1, t_2]$. The proof consists of showing that this is a contradiction. From equation (4.11) it follows that for all $t \in (t_1, t_2]$ the state derivative $\dot{z}(t)$ is strictly positive because all the term in the right hand side are positive. This contradicts the hypothesis and hence proves claim (i). For claims (ii) and (iii), the proof is conducted in four steps. First, the system is shown to be strictly monotonically decreasing in the interval $[0, \tau)$. Next, the system is shown to be strictly monotonically decreasing in the interval $[\tau, 2\tau)$. In a third step, it is shown that the strict monotonic decrease is preserved in all subsequent intervals of length τ . Finally, in step four it is shown that as $t \rightarrow \infty$ both $z(t) \rightarrow 0$ and $\dot{z}(t) \rightarrow 0$.

As a preliminary observation, note that at $t = 0$ equation (4.11) can be written as

$$\begin{aligned}\dot{z}(0) &= az(0)^2 + bz(0) + hc_1z(0) + hc_2z(0)^2 \\ &= (a + hc_2)z(0)^2 + (b + hc_1)z(0)\end{aligned}\tag{4.15}$$

The states that set $\dot{z}(0) = 0$ can be found by finding the roots of the expression

$$0 = (a + hc_2)z(0) \left[\frac{b + hc_1}{a + hc_2} + z(0) \right]\tag{4.16}$$

Hence, the initial states $z(0) = z_1$ and $z(0) = z_2$, where $z_1 = 0$ and $z_2 = -\frac{b+hc_1}{a+hc_2}$ produce zero derivatives at the initial time $t = 0$. The focus now turns to determining conditions that ensure that $z(t)$ is a decreasing function of time. This requires that the condition $\dot{z}(0) < 0$ hold at all finite time.

The first step of the proof considers the interval $t \in [0, \tau)$. Depending on the parameter b , there are two scenarios of relevance. If $b + hc_1 > 0$, then since $z(0) > 0$, it

follows from (4.15) that $\dot{z}(0) > 0$ and the solution is initially increasing. Obviously, this case is not desired. However, if

$$b + hc_1 < 0 \quad (4.17)$$

then from (4.15) it can be concluded that if

$$z(0) < -\frac{b + hc_1}{a + hc_2} \quad (4.18)$$

then $\dot{z}(0) < 0$ and it follows that the solution is initially decreasing. Therefore, in the interval $[0, \tau)$ equation (4.11) can be written in a form similar to that given in Lemma 2, namely,

$$\dot{z}_0(t) = az_0(t)^2 + bz_0(t) + c_0 \quad (4.19)$$

where $c_0 = hc_1z(0) + hc_2z(0)^2$ and where $z_0(t)$ is the solution of (4.11) for $t \in [0, \tau)$. In order to ensure that the equilibrium points of (4.19) are real and distinct the discriminant must satisfy $b^2 - 4ac_0 > 0$, which implies that the system delay must satisfy $h < h_1 := \frac{b^2}{4ac_0}$. Furthermore, since $b + hc_1 < 0$ is the desired condition, it follows that h must also satisfy $h < h_2 := -\frac{b}{c_1}$. This suggests that the system delay must satisfy $h < \min\{h_1, h_2\}$ which yields inequality (4.14) of the lemma. Let $k_1 = \frac{-b - \sqrt{b^2 - 4ac_0}}{2a}$ and $k_2 = \frac{-b + \sqrt{b^2 - 4ac_0}}{2a}$ respectively denote the smallest and largest roots of the right hand side of (4.19). Since $b < 0$, Lemma 2 can be applied to (4.19) to conclude that the solution $z_0(t)$ is strictly monotonically decreasing, and that $z_0(t) \rightarrow k_1$ as $t \rightarrow \infty$ provided that $z(0)$ belongs to the region of attraction $k_1 < z(0) < k_2$. In order to also satisfy the constraint (4.18), the region of convergence is redefined as

$$k_1 < z(0) < \min\left\{-\frac{b + hc_1}{a + hc_2}, k_2\right\} \quad (4.20)$$

which is equivalent to inequality (4.13) in the lemma.

The second step aims to show that $z(t)$ decreases in $[\tau, 2\tau)$. Since it has been established that $z(t)$ decreases in the period $[0, \tau)$, it follows that $\sup_{\tau \leq \theta \leq 2\tau} z(\theta) = z(t - \tau)$ and $\sup_{\tau \leq \theta \leq 2\tau} z(\theta)^2 = z(t - \tau)^2$ in the period $[\tau, 2\tau)$. Hence, for $t \in [\tau, 2\tau)$ equation (4.11) can be written as

$$\dot{z}_\tau(t) = az_\tau(t)^2 + bz_\tau(t) + c(t) \quad (4.21)$$

where

$$c(t) = hc_1 z(t - \tau) + hc_2 z(t - \tau)^2 \quad (4.22)$$

and where $z_\tau(t)$ is the solution of (4.11) when $t \in [\tau, 2\tau)$. Note that as a consequence of the results of the first step of the proof, $c(t)$ is strictly decreasing in $[\tau, 2\tau)$ which implies that the roots of the right hand side of (4.21), namely,

$$K_1(t) = \frac{-b - \sqrt{b^2 - 4ac(t)}}{2a} \quad (4.23)$$

and

$$K_2(t) = \frac{-b + \sqrt{b^2 - 4ac(t)}}{2a}$$

are such that the smaller root $K_1(t)$ is decreasing and the larger roots $K_2(t)$ is increasing. This, in turn, implies that $z(t)$ is strictly decreasing.

The third step involves extending the results of the second step to the subsequent intervals, $[2\tau, 3\tau), [3\tau, 4\tau), \dots$, etc. Let $z_{n\tau}(t)$ represent the solution to system (4.11) in the interval $[n\tau, (n+1)\tau)$ where $n \geq 2$ is an integer. When $t \in [n\tau, (n+1)\tau)$ system (4.11) can be written in the equivalent form

$$\dot{z}_{n\tau}(t) = az_{n\tau}(t)^2 + bz_{n\tau}(t) + c(t)$$

where $c(t)$ is given by (4.22). Note that when $n = 2$, the function $c(t)$ is strictly monotonically decreasing in $t \in [\tau, 2\tau)$. Repeating the argument invoked in the second part of the proof, namely that the monotonicity of $c(t)$ in the interval ensures

that $K_1(t)$ given in (4.23) is strictly monotonically decreasing in that interval, leads to the conclusion that $z_{n\tau}(t)$ is strictly monotonically decreasing in $[n\tau, (n+1)\tau)$ when $n = 2$. The proof is completed by induction for $n = 3, 4, \dots$, etc. Hence, $z_{n\tau}(t)$ is strictly decreasing in any interval of length τ . This implies that $z(t)$ is strictly decreasing which proves claim (ii).

Step four of the proof is based on recognizing that from claim (i) $z(t)$ is bounded from below, and using the fact that $z(t)$ is strictly monotonically decreasing, it follows that $z(t) \rightarrow L$ as $t \rightarrow \infty$, where $L < \infty$ is a limit, and that $\dot{z}(t) \rightarrow 0$. Taking the limit as $t \rightarrow \infty$ on each side of equation (4.21) yields

$$0 = (a + hc_2)L^2 + (b + hc_1)L \quad (4.24)$$

Solving for the two limits of (4.24) yields $L_1 = 0$ and $L_2 = -\frac{b+hc_1}{a+hc_2}$. Now, given that the initial condition (4.13) implies that $z(0) < -\frac{b+hc_1}{a+hc_2} = L_2$, then as $t \rightarrow \infty$, the decreasing state $z(t)$ must reach the lower limit $L_1 = 0$. Thus, $\lim_{t \rightarrow \infty} z(t) = 0$. This proves claim (iii). ■

4.4 Main Result

Now, utilizing the developments in Lemma 3, we are ready to present the main result which concerns the asymptotic stability of the original system (4.1). The approach is to bound the norm of the solution of (4.1) (i.e., $\|x(t)\|$) by a scalar function $z(t)$ that is asymptotically stable. Thus, when $z(t) \rightarrow 0$ then $\|x(t)\| \rightarrow 0$. An argument based on the comparison theorem [41] (see Appendix F) is utilized.

Theorem 1 *The time-delay bilinear system (4.1) under assumptions (A1) and (A2) and the state feedback control law (4.2) is asymptotically stable if*

$$0 < |x(0)| < \min\left\{-\frac{b + hc_1}{a + hc_2}, \frac{-b + \sqrt{b^2 - 4ac_0}}{2a}\right\} \quad (4.25)$$

and

$$h < \min\left\{\frac{b^2}{4a\bar{c}_0}, -\frac{b}{c_1}\right\} \quad (4.26)$$

where $a = \|N\| \|F\|$, $b = \mu(\hat{A})$, $c_1 = \|A_d\bar{A}\| + \|A_dA_d\|$, $c_2 = \|A_dN\| \|F\|$, $c_0 = hc_1|x(0)| + hc_2|x(0)|^2$, $\bar{c}_0 = \frac{c_0}{h}$, and $\hat{A} = \bar{A} + A_d$.

Proof: Since equation (4.3) is continuously differentiable, then

$$x(t) - x(t-h) = \int_{-h}^0 \dot{x}(t+\theta) d\theta \quad (4.27)$$

Substituting for $\dot{x}(t)$ from equation (4.3) and rearranging terms yields the expression

$$x(t-h) = x(t) - \int_{-h}^0 \{ \bar{A}x(t+\theta) + A_dx(t+\theta-h) + Nx(t+\theta)Fx(t+\theta) \} d\theta$$

which can be substituted in equation (4.3) to get

$$\dot{x}(t) = \bar{A}x(t) + A_d[x(t) - \int_{-h}^0 \{ \bar{A}x(t+\theta) + A_dx(t+\theta-h) + Nx(t+\theta)Fx(t+\theta) \} d\theta] + Nx(t)Fx(t)$$

or

$$\dot{x}(t) = \hat{A}x(t) + \int_{-h}^0 (-A_d) \{ \bar{A}x(t+\theta) + A_dx(t+\theta-h) + Nx(t+\theta)Fx(t+\theta) \} d\theta + Nx(t)Fx(t) \quad (4.28)$$

where $\hat{A} = \bar{A} + A_d$. The solution to equation (4.28) has the form

$$\begin{aligned} x(t) = & e^{\hat{A}t}x_0 + \int_0^t e^{\hat{A}(t-s)} \left[\int_{-h}^0 \{ (-A_d)\bar{A}x(s+\theta) - A_d^2x(s+\theta-h) \right. \\ & \left. - A_dNx(s+\theta)Fx(s+\theta) \} d\theta + Nx(s)Fx(s) \right] ds \end{aligned} \quad (4.29)$$

where $x_0 = x(0)$ is the initial condition obtained by setting $x(0) = \Psi(0)$ in equation (4.1). Utilizing the matrix measure property $\|e^{\hat{A}t}\|_p \leq e^{\mu_p(\hat{A}t)}$ [14], and taking the

norm of both sides of equation (4.29) gives

$$|x(t)| \leq e^{\mu(\hat{A})t}|x_0| + \int_0^t e^{\mu(\hat{A})(t-s)} \left[\int_{-h}^0 \{ \|A_d \bar{A}\| |x(s+\theta)| + \|A_d^2\| |x(s+\theta-h)| \right. \\ \left. + \|A_d N\| \|F\| |x(s+\theta)|^2 \} d\theta + \|N\| \|F\| |x(s)|^2 \right] ds$$

Now, the inner integral can be bound using the supremum of its arguments and the length h of the integration interval, to yield

$$|x(t)| \leq e^{\mu(\hat{A})t}|x_0| + \int_0^t e^{\mu(\hat{A})(t-s)} \left[h \|A_d \bar{A}\| \sup_{s-h \leq \theta \leq s} |x(\theta)| + h \|A_d^2\| \sup_{s-2h \leq \theta \leq s-h} |x(\theta)| \right. \\ \left. + h \|A_d N\| \|F\| \sup_{s-h \leq \theta \leq s} |x(\theta)|^2 + \|N\| \|F\| |x(s)|^2 \right] ds$$

Letting $a = \|N\| \|F\|$, $c_1 = \|A_d \bar{A}\| + \|A_d A_d\|$, and $c_2 = \|A_d N\| \|F\|$, and adopting the largest interval $s - 2h \leq \theta \leq s$ gives

$$|x(t)| \leq e^{\mu(\hat{A})t} |x_0| + \int_0^t e^{\mu(\hat{A})(t-s)} \{ hc_1 \sup_{s-2h \leq \theta \leq s} |x(\theta)| \\ + hc_2 \sup_{s-2h \leq \theta \leq s} |x(\theta)|^2 + a |x(s)|^2 \} ds \quad (4.30)$$

Now, let a scalar function with initial condition $z_0 = |x_0|$ satisfy

$$z(t) = e^{\mu(\hat{A})t} z_0 + \int_0^t e^{\mu(\hat{A})(t-s)} \{ hc_1 \sup_{s-2h \leq \theta \leq s} z(\theta) + hc_2 \sup_{s-2h \leq \theta \leq s} z(\theta)^2 + az(s)^2 \} ds$$

so that $|x(t)| \leq z(t)$. Then,

$$\dot{z}(t) = az(t)^2 + \mu(\hat{A})z(t) + hc_1 \sup_{t-2h \leq \theta \leq t} z(\theta) + hc_2 \sup_{t-2h \leq \theta \leq t} z(\theta)^2 \quad (4.31)$$

The system equation (4.31) is of the same form as that of equation (4.11) with $b = \mu(\hat{A})$. Two cases are considered, depending on the norm of the initial condition.

Case 1: $x_0 = x'_0$ where $k_1 < |x_0| < \min\{-\frac{b+hc_1}{a+hc_2}, k_2\}$.

Case 2: $x_0 = x''_0$ where $0 < |x_0| \leq k_1$.

where $k_1 = \frac{-b - \sqrt{b^2 - 4ac_0}}{2a}$ and $k_2 = \frac{-b + \sqrt{b^2 - 4ac_0}}{2a}$. For *case 1*, let the solution to (4.3) be denoted as $x'(t)$ such that inequality (4.30) applies with $x(t) = x'(t)$. Invoking

Lemma 3 show that $z(t) \rightarrow 0$ as $t \rightarrow \infty$. Hence, since $|x'(t)| \leq z(t)$ it follows that $x'(t) \rightarrow 0$ which implies that $x(t)$ is asymptotically stable. For *case 2*, let the solution to (4.3) be denoted as $x''(t)$ such that inequality (4.30) applies with $x(t) = x''(t)$. Since $|x''_0| < |x'_0|$ then from (4.30) it follows that $|x''(t)| \leq |x'(t)|$. Finally, since $x'(t) \rightarrow 0$ then $x''(t) \rightarrow 0$, which implies that the system is asymptotically stable. This completes the proof. ■

4.5 Example

Consider the time-delay bilinear system (4.1) with $h = 0.5$, an initial-state function $\Psi(\phi) = [-1.5 \ 1.5]^T$ for $\phi \in [-2h, 0]$ so that the initial-state vector is $x(0) = [-1.5 \ 1.5]^T$, and the following parameters:

$$A = \begin{bmatrix} 0.5 & -0.2 \\ 0.8 & -2.1 \end{bmatrix}, \quad A_d = \begin{bmatrix} -0.2 & 0 \\ 0.5 & -0.1 \end{bmatrix}, \quad B = \begin{bmatrix} 1 \\ 0 \end{bmatrix}, \quad N = \begin{bmatrix} -0.02 & 0.06 \\ 0.01 & -0.03 \end{bmatrix}$$

Choosing the eigenvalues of \bar{A} to be placed at $\{-1.6, -2.1\}$ yields the feedback matrix $F = [-2.1 \ 0.2]$. Let us investigate the alternative p -norms to verify which norm satisfies the inequality conditions (4.25) and (4.26).

For the 1-norm, neither condition is satisfied. First, the discriminant $D = b^2 - 4ac_0 = -1.8$ and therefore the roots are complex. Second, $h = 0.5 > \{0.36, 0.06\}$. For the 2-norm, both conditions are satisfied. Hence, adopting the 2-norm gives the following values for the parameters in Theorem 1: $a = 0.1492$, $\mu_2(\hat{A}) = b = -1.32$, and $c_0 = 1.4130$. The attraction region (4.25) is given by $0 < |x(0)| = 2.12 < \min\{3.8, 7.6\}$. Also, the bound on the delay is given by $h = 0.5 < \min\{1.18, 1.03\}$. Finally, for the ∞ -norm, both conditions are satisfied. The values of the parameters in Theorem 1 are given by: $a = 0.168$, $\mu_\infty(\hat{A}) = b = -1.8$, and $c_0 = 1.0415$. The delay-bound condition equation (4.26) is satisfied since $h = 0.5 < \min\{1.44, 2.3148\}$. Furthermore, the domain of attraction (4.25) is given by $0 < |x(0)| = 1.5 < \min\{5.4855, 10.1\}$.

Figures 4.2 and 4.3 illustrate the results of a simulation study. Figure 4.2 depicts the time evolution of the state trajectories which assume an asymptotic behavior. Figure 4.3 shows the norm of $x(t)$ converging to the origin.

Remark 3 *The sufficient conditions given in (4.25) and (4.26) can vary depending on the norm and matrix measure chosen. While stability can be concluded for a certain norm, it may not be so for other norms. The stability conditions can, however, be tightened and therefore reducing conservatism by selecting other norms and matrix measures. One choice could be the following:*

$$\|A\|_w = \max_i \sum_j \frac{w_j}{w_i} |a_{ij}|$$

and

$$\mu_w(A) = \max_i \{a_{ii} + \sum_{j \neq i} \frac{w_j}{w_i} |a_{ij}|\}$$

4.6 Conclusions

Delay-dependent stability conditions are derived for a class of time-delay bilinear systems utilizing the comparison theorem and matrix measure techniques. The sufficient stability conditions provide a bound for the tolerable system delay as well as the domain of attraction for which asymptotic stability is guaranteed. These results are however conservative mainly due to applying a supremization over a large time interval which is twice the size of the delay.

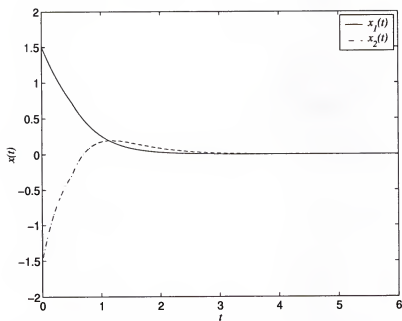


Figure 4.2: Plot of the trajectories of the system states.

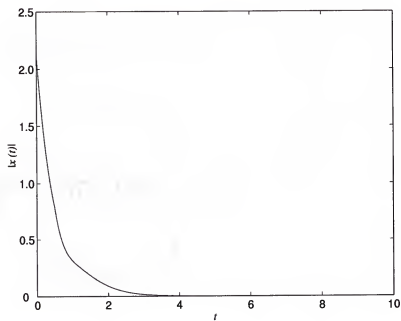


Figure 4.3: Plot of the trajectories of the system states.

4.7 Further Analysis of the System in Lemma 1

Further analysis of the system equation (4.4), and a discussion of the behavior of its solution (4.5) is presented in this section.

Theorem 2 *Given the system (4.4) and the analytic solution (4.5), then the following observations are readily verified:*

Case 1: $b > 0$

$$\lim_{t \rightarrow \infty} y(t) = \begin{cases} \infty & \text{if } y(0) > 0 \\ 0 & \text{if } y(0) = 0 \\ -\frac{b}{a} & \text{if otherwise} \end{cases} \quad \begin{matrix} (4.32a) \\ (4.32b) \\ (4.32c) \end{matrix}$$

Case 2: $b < 0$

$$\lim_{t \rightarrow \infty} y(t) = \begin{cases} 0 & \text{if } y(0) < -\frac{b}{a} \\ -\frac{b}{a} & \text{if } y(0) = -\frac{b}{a} \\ \infty & \text{if otherwise} \end{cases} \quad \begin{matrix} (4.33a) \\ (4.33b) \\ (4.33c) \end{matrix}$$

Proof: For Case 1, it is noted from (4.5) that the solution becomes unbounded at finite time when the denominator is zero. The finite escape time (FET) can be calculated as a function of the parameters a , b , and $y(0)$, by setting the denominator to zero and solving for t . The result is

$$t_{FET} = \frac{1}{b} \ln \left[1 + \frac{b}{ay(0)} \right] \quad (4.34)$$

Now, to prove the first branch of Case 1, namely (4.32a), the denominator of (4.5) is set to zero, *i.e.*,

$$b + ay(0)(1 - e^{bt}) = 0$$

or

$$1 + \frac{a}{b} y(0) (1 - e^{bt}) = 0 \quad (4.35)$$

Now, since as $t \rightarrow \infty$ the quantity $1 - e^{bt}$ takes values between zero and $-\infty$, and since $\frac{a}{b}y(0) > 0$, then the equality (4.35) is satisfied for some $t > 0$. Hence, the denominator becomes zero and the solution blows up at finite time. The second branch of Case 1 (4.32b) is readily verified by substituting $y(0) = 0$ in (4.5). Finally, substituting for $y(0) = -\frac{b}{a}$ into (4.5) gives $y(t) = -\frac{b}{a}$, which proves the branch (4.32c). Graphs (a) and (b) of Figure 4.4 show the derivative graph and the solution curves of (4.4), respectively, for the case where $b > 0$.

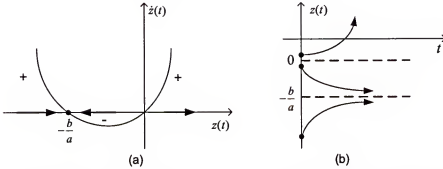


Figure 4.4: Graphical interpretation of the differential equation(4.4) for the case where $b > 0$: (a) derivative graph, (b) solution curves

For Case 2, the first branch (4.33a) indicates that the system is asymptotically stable when the initial condition satisfies $y(0) < -\frac{b}{a}$. Therefore, in this case the finite escape time is avoided. To verify this claim, consider the denominator expression (4.35). For $t > 0$ the quantity $1 - e^{bt}$ takes values in the interval $(0, 1)$. The goal is to show that for $y(0) < -\frac{b}{a}$ the equality (4.35) is never satisfied. First, it is trivial to verify this claim for $y(0) = 0$. Second, for $0 < y(0) < -\frac{b}{a}$ it follows that, since $-1 < \frac{a}{b} y(0) < 0$, the second term in (4.35) is never equal to 1. Finally, for $y(0) < 0$, equality (4.35) is again never satisfied since its second term in is always positive. This proves the first branch of Case 2. The second branch (4.33b) is readily verified by substituting $y(0) = -\frac{b}{a}$ in (4.4). Finally, branch (4.33c) indicates that

for $y(0) > -\frac{b}{a}$ there is a finite escape time, which means that (4.35) is satisfied for some finite values of t . First, note that $-1 < \frac{a}{b} y(0)$. Next, since the values of the quantity $1 - e^{bt}$ belongs to the interval $(0, 1)$, then for some time $t > 0$ the second term in (4.35) can equal -1 such that (4.35) is satisfied. This completes the proof of Case 2. Figure 4.5 depicts the solution behavior for the case where $b < 0$. It is clear that when $y(0) < -\frac{b}{a}$ the solution converges asymptotically to the origin, and for $y(0) > -\frac{b}{a}$ the system becomes unstable.

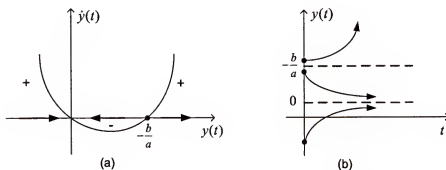


Figure 4.5: Graphical interpretation of the differential equation(4.4) for the case where $b < 0$: (a) derivative graph, (b) solution curves

CHAPTER 5

FUTURE WORK AND DISCUSSIONS

Future work may focus on three problems. First, designing a sliding mode controller for a class of time-delay bilinear systems. Second, extending the concept of the Nyquist robust sensitivity margin (NRSM) to a class of uncertain systems with multilinear uncertainty structure. Finally, the concept of the NRSM can be utilized to obtain a weighting function for an H_∞ design similar to work by Baowei [?].

5.1 Problem 1 : Sliding Mode Control for a Delayed Bilinear System

The system under consideration is of the form

$$\begin{aligned}\dot{x}(t) &= Ax(t) + A_d x(t-h) + Bu(t) + Nx(t)u(t) \\ x(\tau) &= \Phi(\tau), \quad \tau \in [-h, 0]\end{aligned}\tag{5.1}$$

where the system delay h is assumed constant.

The objective is to design a sliding mode control (SMC) that renders the system asymptotically stable. However, when nonlinearity is combined with time-delay, the problem becomes more challenging from the control design viewpoint as well as from the perspective of the stability analysis. Therefore, problems may arise when designing a controller to force the trajectories into the sliding manifold and to ensure they stay there for all subsequent time.

5.2 Problem 2 : Extending the NRSM

Multilinear Uncertainty. An interesting, yet challenging, problem is to extend the concept of the *Nyquist robust sensitivity margin* to include linear system

with multilinear uncertainty structure, *i.e.*, systems of the form

$$g(s) = \frac{n(s, q)}{d(s, r)} \quad (5.2)$$

where r and q are multilinear vectors. In the polynomial case, since the multilinear uncertainty lacks edge results, the mapping theorem [7] introduces overbounding polynomials which of course can be conservative. For the transfer function (5.2), there are two situations. First, when the vectors r and q are independent, stability can be analyzed using the mapping theorem by considering a polytopic family $\bar{g}(s)$ such that any worst-case margin calculated for $\bar{g}(s)$ is considered a guaranteed margin for $g(s)$ [7]. However, when the vectors r and q depend on each other, then there are no comparable results to analyze the robust stability of the system.

H- ∞ Design. Another future work project is to design an H- ∞ controller based on a weight function derived from $k_{N,s}$. This project can follow the work of Baowei [29, 30] which is summarized as follow. Given the system in Figure 5.1, use of made of the $M - \Delta$ structure given in Figure 5.2 where it is known from the small gain theory [57] that the system in Figure xx is internally stable for any $\Delta(s)$ satisfying

$$\|\Delta(s)\|_{\infty} < \frac{1}{\|M(s)\|_{\infty}}$$

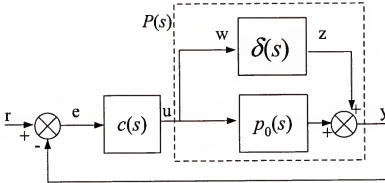


Figure 5.1: The negative feedback loop of the uncertain system $p(s)$ with a controller $c(s)$.

The transformation of the system in Figure 5.1 into the $M - \Delta$ formulation is given in Figure 5.3 where it follows that the system is stable for any $\delta(s)$ satisfying

$$\|\delta(s)\|_{\infty} < \frac{1}{\|R(s)\|_{\infty}} \quad (5.3)$$

where $R(s) = \frac{c(s)}{1+c(s)p_0(s)}$. Next, the system in Figure 5.3 is put into the mixed sensitivity framework where the stability conditions can be expressed by the inequality

$$\|W_2(s)R(s)\|_{\infty} < 1 \quad (5.4)$$

The problem now is to choose $W_2(s)$ to represent the effective part of $\delta(s)$. Finally, a weighting scheme, namely the *effective critical perturbation radius* (ECPR), is designed based on the critical direction theory.

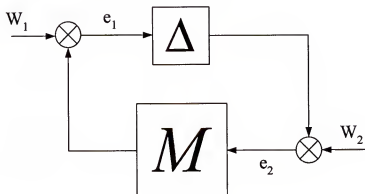


Figure 5.2: The standard $M - \Delta$ loop for stability analysis.

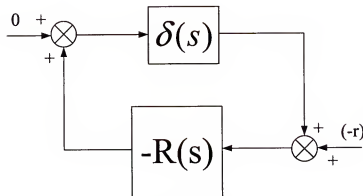


Figure 5.3: A system with parametric uncertainty in the standard $M - \Delta$ loop.

APPENDIX A DERIVATION FOR THE REACHING TIME

General case

Consider a Lyapunov function $V(t) = \frac{1}{2}s(t)^2$. The standard condition that ensures reaching the sliding manifold in finite time is given by

$$\dot{V}(t) = s(t)\dot{s}(t) \leq -\eta|s(t)| \quad (\text{A.1})$$

where $\eta > 0$ [49].

Theorem 1 *Under the inequality given in (A.1), the time at which the sliding manifold is reached is given by*

$$t_s = \frac{1}{\eta}|s_0| \quad (\text{A.2})$$

Proof: The proof utilizes Figure A.1. From the figure it is noted that the initial value of the sliding function is $s(0)$, and that $s(t_s) = 0$. The equality limit of (A.1) (i.e., $s(t)\dot{s}(t) = -\eta|s(t)|$) can be written as

$$dt = -\frac{1}{\eta} \frac{s}{|s(t)|} ds \quad (\text{A.3})$$

where $s(t) \neq 0$. The reaching time t_s is obtained by integrating (A.3) as follows:

$$\int_0^{t_s} dt = -\frac{1}{\eta} \int_0^{t_s} \frac{|s(t)|}{s(t)} ds$$

which yields the result

$$t_s = \begin{cases} -\frac{1}{\eta}(s(t_s) - s(0)) & : s(t) > 0, \text{ case}(a) \\ -\frac{1}{\eta}(-s(t_s) + s(0)) & : s(t) < 0, \text{ case}(b) \end{cases} \quad (\text{A.4})$$

Since $s(t_s) = 0$, equation (A.4) can be written as

$$t_s = \begin{cases} \frac{1}{\eta} s(0) \\ -\frac{1}{\eta} s(0) \end{cases}$$

or

$$t_s = \frac{1}{\eta} |s(0)|$$

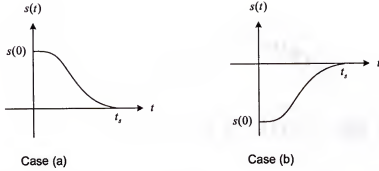


Figure A.1: Plot of the switching function for $s(0) > 0$ (a), and $s(0) < 0$ (b).

New condition

Consider the Lyapunov condition

$$\dot{V}(t) = -\rho|s|^2 - d|s| \quad (\text{A.5})$$

where $\rho > 0$ and $d > 0$. Using the fact that $|s(t)| = \sqrt{2V}$, equation (A.5) can be rewritten as

$$\dot{V}(t) = -2\rho V(t) - \sqrt{2}dV(t)^{0.5} \quad (\text{A.6})$$

Let $y(t)^2 = V(t)$. Then equation (A.6) becomes

$$\dot{V}(t) = 2y(t)\dot{y}(t) = -2\rho y(t)^2 - \sqrt{2}d y(t) \quad (\text{A.7})$$

or

$$\dot{y}(t) + \rho y(t) = -\frac{1}{\sqrt{2}}d$$

Multiplying through by $e^{\rho t}$ and rearranging terms yields

$$\frac{d}{dt}(y(t)e^{\rho t}) = -\frac{d}{\sqrt{2}}e^{\rho t} \quad (\text{A.8})$$

Integrating both sides of (A.8) gives

$$y(t)e^{\rho t} = -\frac{d}{\sqrt{2}\rho}e^{\rho t} + c \quad (\text{A.9})$$

The constant c can be found by evaluating (A.9) at $t = 0$, which gives

$$c = y(0) + \frac{d}{\sqrt{2}\rho}$$

Substituting for the constant c , equation (A.9) can be written as

$$y(t) = e^{-\rho t}[y(0) + \frac{d}{\sqrt{2}\rho}] - \frac{d}{\sqrt{2}\rho} \quad (\text{A.10})$$

Now, using (A.6) equation (A.10) can be written as

$$\sqrt{V(t)} = e^{-\rho t}[\sqrt{V(0)} + \frac{d}{\sqrt{2}\rho}] - \frac{d}{\sqrt{2}\rho}$$

Since at sliding mode $V(t) = \sqrt{V(t)} = 0$ because $s(t) = \dot{s}(t) = 0$, it then follows that

$$0 = -\rho t_s + \ln[\sqrt{V(0)} + \frac{d}{\sqrt{2}\rho}] - \ln \frac{d}{\sqrt{2}\rho}$$

or

$$t_s = \frac{1}{\rho} \ln[1 + \frac{\sqrt{2}\rho\sqrt{V(0)}}{d}] \quad (\text{A.11})$$

Now, since $V(t) = \frac{1}{2}s(t)^T s(t)$, it follows that

$$t_s = \frac{1}{\rho} \ln[1 + \frac{\sqrt{2}\rho\sqrt{\frac{s(0)^T s(0)}{2}}}{d}]$$

■

APPENDIX B DERIVATION OF THE BOUND ON $v(t)$ OF CHAPTER 3

This appendix presents a derivation of the bound (3.14)

$$|v(t)| \leq \eta(h)|z(t)|$$

Consider the equation

$$v(t) = \int_{t-h}^t e^{A(t-h-\tau)} B_d u(\tau) d\tau \quad (\text{B.1})$$

Substituting for the control law $u(t) = -Fz(t)$ valid at sliding mode and taking the norm of both sides of (B.1) yields

$$|v(t)| \leq \int_{t-h}^t \|e^{A(t-h-\tau)}\| \|B_d\| \|F\| |z(\tau)| d\tau \quad (\text{B.2})$$

Let $\theta = -(t-h-\tau)$. Then for $\tau = t$, $\theta = h$, and for $\tau = t-h$, $\theta = 0$. The inequality (B.2) then implies

$$\begin{aligned} |v(t)| &\leq \int_0^h \|e^{-A\theta}\| \|B_d\| \|F\| \max_{t-h \leq \psi \leq t} |z(\psi)| d\theta \\ &\leq h \max_{0 \leq \theta \leq h} \|e^{-A\theta}\| \|B_d\| \|F\| \bar{z}(t, t-h) \end{aligned} \quad (\text{B.3})$$

where $\bar{z}(t, t-h) = \max_{t-h \leq \psi \leq t} |z(\psi)|$. Utilizing the Razumikhin concept [38], it follows that

$$\bar{z}(t, t-h) \leq \alpha |z(t)|$$

where α is a Razumikhin parameter. Therefore, inequality (B.3) can be written as

$$|v(t)| \leq h \max_{0 \leq \theta \leq h} \|e^{-A\theta}\| \|B_d\| \|F\| \alpha |z(t)| \quad (\text{B.4})$$

which yields the bound $|v(t)| \leq \eta(h)|z(t)|$, where η represent the right-hand side of inequality (B.4).

APPENDIX C SOLUTION FOR A DIFFERENTIAL EQUATION

Here, the derivation of the solution (4.5) of the system equation (4.4) given in Lemma 1 of Chapter 4 is presented.

Theorem 1 *Consider the scalar differential equation*

$$\dot{x}(t) = ax(t)^2 + bx(t) \quad (\text{C.1})$$

then the analytic solution is given by

$$x(t) = \frac{be^{bt} x(0)}{b + a x(0) (1 - e^{bt})} \quad (\text{C.2})$$

Proof: Equation (C.1) can be written as

$$\frac{dx}{bx(t) + ax(t)^2} = dt \quad (\text{C.3})$$

Integrating both sides gives

$$\int \frac{dx}{x(t)(ax(t) + b)} = t + c_1$$

where c_1 is the integration constant. Working out the integral yields

$$\frac{1}{b} \ln\left[\frac{x(t)}{ax(t) + b}\right] = t + c_1$$

which after multiplying through by b , and taking the exponential of both sides gives

$$\frac{x(t)}{ax(t) + b} = e^{bt} e^{bc_1} = e^{bt} c_2 \quad (\text{C.4})$$

where $c_2 = e^{bc_1}$. At $t = 0$, the constant $c_2 = \frac{x(0)}{ax(0)+b}$. Substituting back into (C.4), and re-arranging terms yields

$$x(t)[ax(0) + b] = e^{bt}x(0)[ax(t) + b]$$

Finally, solving for $x(t)$ gives the solution

$$x(t) = \frac{be^{bt} x(0)}{b + a x(0) (1 - e^{bt})}$$

■

APPENDIX D PROOF OF CLAIMS (i) & (ii) OF LEMMA 1 OF CHAPTER 4

For convenience we rewrite the system equation of Lemma 1. Given the scalar differential equation

$$\dot{y}(t) = ay(t)^2 + by(t) \quad (\text{D.1})$$

where $a > 0$ and $b < 0$. Its analytic solution is given in Appendix C and can be written as

$$y(t) = \frac{e^{bt} y(0)}{1 + \frac{a}{b} y(0) (1 - e^{bt})} \quad (\text{D.2})$$

Now, for the initial condition bound $0 < y(0) < -\frac{b}{a}$, we need to prove the following two claims:

Claim (i) : $y(t) > 0 \forall t < \infty$.

Claim (ii) : $y(t+T) < y(t) \forall t < T < \infty$.

Claim (i) can be checked by verifying that both the numerator and the denominator of (D.2) are either positive or negative. Let's consider the numerator first. Since the exponential function is always positive (*i.e.*, $e^{bt} > 0$), and $y(0) > 0$, then the numerator is positive. Now, for the denominator, since $0 < y(0) < -\frac{b}{a}$ then it can be readily verified that

$$-1 < \frac{a}{b} y(0) < 0 \quad (\text{D.3})$$

Furthermore, using the fact that $0 \leq 1 - e^{bt} < 1 \forall t \geq 0$ it follows that

$$0 > \frac{a}{b} y(0) (1 - e^{bt}) > -1 \quad (\text{D.4})$$

Therefore, the denominator of (D.2) is easily seen to be positive. Hence, $y(t) > 0 \forall t < \infty$. This completes the proof of claim (i).

Claim (ii) implies that the solution is strictly monotonically decreasing. It can be checked by verifying that the ratio $R < 1$, where

$$R = \frac{y(t+T)}{y(t)} \quad (\text{D.5})$$

is satisfied for all $t < T < \infty$. Using (D.2), the ratio (D.5) can be written as

$$R = \frac{e^{b(t+T)}}{1 + \frac{a}{b}y(0)(1 - e^{b(t+T)})} \cdot \frac{1 + \frac{a}{b}y(0)(1 - e^{bt})}{e^{bt}}$$

which after simple manipulations reduces to

$$R = \frac{e^{bT}[1 + \frac{a}{b}y(0)(1 - e^{bt})]}{1 + \frac{a}{b}y(0)(1 - e^{bt}e^{bT})} \quad (\text{D.6})$$

Multiplying the numerator and the denominator of (D.6) through gives

$$R = \frac{e^{bT} + e^{bT}\frac{a}{b}y(0) - e^{bT}e^{bt}\frac{a}{b}y(0)}{1 + \frac{a}{b}y(0) - e^{bT}e^{bt}\frac{a}{b}y(0)} \quad (\text{D.7})$$

Ignoring the last term in the numerator and denominator of (D.7) since they are the same, then the truncated ration R' is given by

$$R' = \frac{e^{bT}(1 + \frac{a}{b}y(0))}{1 + \frac{a}{b}y(0)} = e^{bT} < 1 \quad (\text{D.8})$$

for all $T > 0$. This shows that $R < 1$, and hence, proves claim (ii) of Lemma 1.

APPENDIX E MATRIX MEASURE

The following definition of the matrix measure and its properties are found in Vidysagar [52].

Definition 1 *The matrix measure, also known as the logarithmic derivative, of an induced-matrix norm $\|\cdot\|_p$ on $C^{n \times n}$ is a function $\mu_p : C^{n \times n} \rightarrow \mathcal{R}$ defined by*

$$\mu_p(A) = \lim_{\epsilon \rightarrow \infty} \frac{\|I + \epsilon A\|_p - 1}{\epsilon} \quad (\text{E.1})$$

The matrix measure of $A \in C^{n \times n}$ corresponding to the 1, 2, and ∞ norms is given, respectively, by

$$\begin{aligned} \mu_{p1}(A) &= \max_j \{a_{jj} + \sum_{p \neq j} |a_{pj}|\} \\ \mu_{p2}(A) &= \lambda_{\max}[(A^* + A)]/2 \\ \mu_{p\infty}(A) &= \max_p \{a_{pp} + \sum_{j \neq p} |a_{pj}|\} \end{aligned}$$

Some useful properties of matrix measure include the following:

- $\mu_p(A + B) = \mu_p(A) + \mu_p(B)$.
- $-\mu_p(-A) \leq \text{Re } \lambda \leq \mu_p(A)$ where λ is an eigenvalue of A .
- $\mu_p(\cdot)$ is a convex function on $C^{n \times n}$.

APPENDIX F THE COMPARISON THEOREM

Let a vector-valued function $v(t, s, z) : J \times J \times \mathbb{R}^m \rightarrow \mathbb{R}^m$, $J := [t_0, \infty]$ has the following property. For any fixed t, s ,

$$z_1 \leq z_2 \rightarrow v(t, s, z_1) \leq v(t, s, z_2)$$

Let $z(t)$ be the solution to the inequality

$$z(t) \leq z(0) + \int_{t_0}^t v(t, s, z(s-h)) \, ds$$

Then the maximal solution $r(t)$ of

$$w(t) \leq z(0) + \int_{t_0}^t v(t, s, w(s-h)) \, ds$$

satisfies $z(t) \leq r(t)$ for $t \geq t_0$.

REFERENCES

- [1] Z. Artstein. Linear systems with delayed controls: A reduction. *IEEE Transactions on Automatic Control*, AC-27:869–879, 1982.
- [2] C. T. Baab, J. C. Cockburn, H. A. Latchman, and O. D. Crisalle. Generalization of the nyquist robust stability margin and its applications to system with real affine parametric uncertainties. *International Journal of Robust and Nonlinear Control*, 11:1415–1434, 2001.
- [3] B. R. Barmish. A generalization of Kharitonov’s four-polynomial concept for robust stability problems with linearly dependent coefficient perturbations. *IEEE Transactions on Automatic Control*, 34:157–165, 1989.
- [4] B. R. Barmish. *New Tools for Robustness of Linear Systems*. McMillan, New York, 1994.
- [5] G. Bartolini. Chatteing phenomena in discontinuous control systems. *International Journal of Systems Science*, 30(12):2471–2481, 1989.
- [6] V. R. Basker, K. Hrissagis, and O. D. Crisalle. Variable structure control design for reduced chatter in uncertain time delay systems. In *Proc. 36th IEEE Conference on Decision and Control*, volume 4, pages 3234–3236, 1997.
- [7] S. P. Bhattacharyya. *Robust Control—The Parametric Approach*. Prentice-Hall, New Jersey, 1995.
- [8] H. Chapellat and S. Bhattacharyya. A generalization of Kharitov’s theorem: Robust stability of interval plants. *IEEE Transactions on Automatic Control*, 34:306–311, 1989.
- [9] H. Chapellat, M. Dahleh, and S. Bhattacharyya. On robust nonlinear stability of interval control systems. *IEEE Transactions on Automatic Control*, 36:59–67, 1991.
- [10] M. S. Chen. Exponential stabilization of a constrained bilinear system. *Automatica*, 34:989–992, 1998.
- [11] M. S. Chen and Y. Z. Chen. Normalised quadratic controls for a class of bilinear systems. In *IEE Proceedings on Control Theory Application*, volume 149, pages 520–524, 2002.

- [12] M. S. Chen and S. T. Tsao. Exponential stabilization of a class of unstable bilinear system. *IEEE Transactions of Automatic Control*, 45:989–992, 2000.
- [13] C. Chiang and F. Kung. Stability analysis of continuous bilinear systems. *Journal of the Chinese Institute of Engineers*, 17:569–576, 1994.
- [14] W. A. Coppel. *Stability and Asymptotic Behavior of Differential Equations*. Health, Boston, 1965.
- [15] T. Cormen, C. Leiserson, and R. Rivest. *Introductoin to Algorithms*. McGraw-Hill, New York, 1990.
- [16] R. A. DeCarlo, S. H. Zak, and G. P. Matthews. Variable structure control of nonlinear multivariable systems: A tutorial. In *Proceedings of the IEEE*, volume 76, pages 212–232, 1988.
- [17] J. Doyle. Analysis of feedback systems with structured uncertainties. In *IEE Proceedings Part D*, volume 129, pages 242–250, 1982.
- [18] L. Dugard and E. I. Verriest. *Stability and Control of Time-Delay Systems*. Springer-Verlag, London, 1998.
- [19] D. L. Elliott. Bilinear systems. *Wiley Encyclopedia of Electrical Engineering*, 2:308–323, 1999.
- [20] D. Feiqi, L. Youngqing, and F. Zhaoshu. Variable structure control of time-delay systems with retarded state and retarded control. In *IEEE International Conference on Systems, Man and Cybernetics*, volume 1, pages 102–106, 1996.
- [21] M. Fu. Computing the frequency response of linear systems with parametric perturbations. *Systems & Control Letters*, 15:45–52, 1990.
- [22] F. Gouaisbaut, W. Perruquetti, and J. P. Richard. A sliding mode control for linear systems with input and state delays. In *Proceedings of the 38th IEEE Conference on Decision and Control*, volume 4, pages 4234–4239, 1999.
- [23] J. Guojun and S. Wenzhong. Stability of bilinear time-delay systems. *IMA Journal of Mathematical Control and Information*, 18:53–60, 2001.
- [24] D. W. Ho, G. Lu, and Y. Zheng. Global stabilisation for bilinear systems with time delay. volume 149, pages 89–94, 2002.
- [25] K. J. Hu, V. R. Basker, and O. D. Crisalle. Sliding mode control of uncertain input-delay systems. In *Proc. of the Americal Control Conference*, volume 1, pages 564–568, 1998.
- [26] J. Y. Hung, W. Gao, and J. C. Hung. Variable structure control : A survey. *IEEE Transactions on Indusrial Electronics*, 40(1):2–21, 1993.

- [27] S. R. Inamdar, V. R. Kumar, and N. D. Kulkarni. Dynamics of reacting systems in the presence of time-delay. *Chemical Engineering Science*, 46(3):901–908, 1991.
- [28] E. M. Jafarov. Design of sliding mode control for multi-input systems with multiple state delays. In *Proc. of the American Control Conference*, volume 2, pages 1139–1143, 2000.
- [29] B. Ji, H. A. Latchman, and O. D. Crisalle. Interpretation of static-weight \mathcal{H} -infinity design approaches for interval plants. In *Proc. of the 41st IEEE Conference on Decision and Control*, volume 2, pages 1434–1439, 2002.
- [30] B. Ji, H. A. Latchman, and O. D. Crisalle. Robust H-infinity stabilization for interval plants. In *IEEE Conference Control Applications/Computer Aided Control System Design*, volume 2, pages 1112–1117, 2002.
- [31] H. Khalil. *Nonlinear Systems*. Prentice-Hall, Inc., New Jersey, 1996.
- [32] J. Kharitonov. Asymptotic stability of an equilibrium position of a family of systems of linear differential equations. *Differential Equations*, 14:1483–1485, 1979.
- [33] A. J. Koshkouei and A. S. Zinober. Sliding mode time-delay systems. In *IEEE International Workshop on Variable Structure Control*, pages 97–101, 1996.
- [34] D. Krupp and Y. B. Shtessel. Chattering-free sliding mode control with unmodeled dynamics. In *Proceedings of the American Control Conference*, volume 1, pages 530–534, 1999.
- [35] H. A. Latchman and O. D. Crisalle. Exact robustness analysis for highly structured frequency domain uncertainties. In *Proc. of American Control Conference*, volume 6, pages 3982–3987, 1995.
- [36] H. A. Latchman, O. D. Crisalle, and V. R. Basker. The Nyquist robust stability margin- A new metric for the stability of uncertain systems. *International Journal of Robust and Nonlinear Control*, 7:211–226, 1997.
- [37] P. Liu and H. Hung. Stability for bilinear time-delay systems with saturating actuators. In *IEEE Proc. of International Symposium on Industrial Electronics*, volume 3, pages 1082–1086, 1999.
- [38] M. S. Mahmoud. *Robust Control and Filtering for Time-Delay Systems*. Marcel Dekker, Inc., New York, 1996.
- [39] R. R. Mohler. *Bilinear Control Processes*. McGraw-Hill, New York, 1973.
- [40] R. R. Mohler. *Nonlinear Systems: Application to Bilinear Control*. Prentice-Hall, New Jersey, 1991.

- [41] T. Mori, N. Fukuma, and M. Kuwahara. Simple stability criteria for single and composite linear systems with time delays. *International Journal of Control*, 34:1175–1184, 1981.
- [42] S. Niculescu, S. Tarbouriech, J. Dion, and L. Dugard. Stability criteria for bilinear systems with delayed state and saturating actuators. In *Proceedings of the 34th IEEE Conference on Decision and Control*, volume 2, pages 2064–2069, 1995.
- [43] S. Oucheriah. Dynamic compensation of uncertain time-delay systems using variable structure approach. *IEEE Transactions on Circuits And Systems: Fundamental Theory and Applications*, 42(8):466–469, 1995.
- [44] M. Poljak and J. Rohn. Checking robust nonsingularity is np-hard. *Mathematics of Control, Signals, and Systems*, 6:1–9, 1993.
- [45] Y. Roh and J. Oh. Sliding mode control with uncertainty adaptation for uncertain input-delay systems. In *Proc. of the American Control Conference*, volume 1, pages 636–640, 2000.
- [46] M. G. Safonov. Stability margins of diagonally perturbed multivariable feedback systems. In *IEE Proceedings Part D*, volume 129, pages 251–256, 1982.
- [47] K. Shyu and J. Yan. Robust stability of uncertain time-delay systems and its stabilization by variable structure control. *International Journal of Control*, 57(1):237–246, 1993.
- [48] A. Sideris. An efficient algorithm for checking the robust stability of a polytope of polynomials. *Math. Control Signals & Systems*, 4:315–337, 1991.
- [49] J. E. Slotine. Sliding controller design for non-linear systems. *International Journal of Control*, 40(2):421–434, 1984.
- [50] J. E. Slotine and W. Li. *Applied Nonlinear Control*. Printice-Hall, Inc., New Jersey, 1991.
- [51] V. Utkin. Variable structure systems with sliding modes. *IEEE Transactions on Automatic Control*, AC-22(2):212–222, 1977.
- [52] M. Vidysagar. *Nonlinear Systems Analysis*. Prentice-Hall, New Jersey, 1978.
- [53] L. Wang. Robust strong stabilizability of interval plants: It suffices to check two vertices. *Systems & Control Letters*, 26:133–136, 1995.
- [54] L. Wang. Kharitonov-like theorems for robust performance of interval systems. *Journal of Mathematical Analysis Applications*, 279:430–441, 2003.

- [55] Y. Xia, J. Han, and Y. Jia. A sliding mode control for linear systems with input and state delays. In *Proceedings of the 41st IEEE Conference on Decision and Control*, volume 3, pages 3332–3337, 2002.
- [56] K. D. Young, V. Utkin, and U. Ozguner. A control engineer's guide to sliding mode control. *IEEE Transactions on Control Systems Technology*, 7(3):328–342, 1999.
- [57] K. Zhou, J. Doyle, and K. Glover. *Robust and Optimal Control*. Prentice-Hall, New Jersey, 1996.

BIOGRAPHICAL SKETCH

Saleh Al-Shamali was born in Kuwait City in 1973. He obtained his bachelor's degree in electrical and computer engineering at the University of Missouri-Columbia in December 1996. He worked for a year at Kuwait Oil Company (KOC) as a technical engineer. In 1998, he decided to pursue a master's and Ph.D. degree in the controls and systems area. He joined the Electrical and Computer Engineering Department at the University of Florida in Fall 1998. He is aiming to graduate in December 2004.

STABILITY ANALYSIS AND CONTROL DESIGN FOR UNCERTAIN AND TIME-DELAY SYSTEMS

Saleh A. Al-Shamali

(352) 392-2584

Department of Electrical and Computer Engineering

Chair: Haniph A. Latchman

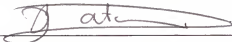
Cochair: Oscar D. Crisalle

Degree: Doctor of Philosophy

Graduation Date: December 2004

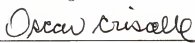
This dissertation develops methodologies that enable analysis and control design for real linear and bilinear systems subject to uncertainty and time delay. An indicator for the robust stability of uncertain systems is proposed, namely, the *Nyquist Robust Sensitivity Margin*, a tool indicates how large a parameter perturbation can be before causing instability. Moreover, new control designs to stabilize linear and bilinear systems under the influence of time-delay are proposed. A *sliding mode control* law is designed to stabilize a linear plant affected by time delay. Also, a state feedback control is proposed to stabilize a time-delay bilinear system. The results obtained by the two designs provide quantitative information regarding the largest delay the plant can handle.

I certify that I have read this study and that in my opinion it conforms to acceptable standards of scholarly presentation and is fully adequate, in scope and quality, as a dissertation for the degree of Doctor of Philosophy.



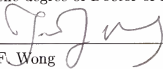
Haniph A. Latchman, Chair
Professor of Electrical and Computer Engineering

I certify that I have read this study and that in my opinion it conforms to acceptable standards of scholarly presentation and is fully adequate, in scope and quality, as a dissertation for the degree of Doctor of Philosophy.



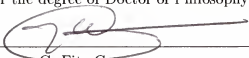
Oscar D. Crisalle, Cochair
Professor of Chemical Engineering

I certify that I have read this study and that in my opinion it conforms to acceptable standards of scholarly presentation and is fully adequate, in scope and quality, as a dissertation for the degree of Doctor of Philosophy.



Tan F. Wong
Assistant Professor of Electrical and Computer Engineering


I certify that I have read this study and that in my opinion it conforms to acceptable standards of scholarly presentation and is fully adequate, in scope and quality, as a dissertation for the degree of Doctor of Philosophy.



Norman G. Fitz-Coy
Associate Professor of Mechanical and Aerospace Engineering

This dissertation was submitted to the Graduate Faculty of the College of Engineering and to the Graduate School and was accepted as partial fulfillment of the requirements for the degree of Doctor of Philosophy.

December 2004



Pramod P. Khargonekar
Dean, College of Engineering

Kenneth J. Gerhardt
Interim Dean, Graduate School